

Status of global fits to neutrino oscillations

M. M. Altoni,¹ T. Schwetz,^{2,y} M. A. Tortola,^{3,z} and J. W. F. Valle^{3,x}

¹C N. Yang Institute for Theoretical Physics, SUNY at Stony Brook,
Stony Brook, NY 11794-3840, USA

²Physik Department, Technische Universität München,
James-Franck-Strasse, D-85748 Garching, Germany

³AHEP Group, Instituto de Física Corpuscular (C.S.I.C./Universitat de Valencia
Edificio Institutos de Paterna, Apt 22085, E-46071 Valencia, Spain

Abstract

We review the present status of global analyses of neutrino oscillations, taking into account the most recent neutrino data and state-of-the-art solar and atmospheric neutrino flux calculations. We give the two-neutrino solar + KamLAND results, as well as two-neutrino atmospheric + K2K oscillation regions, discussing in each case the robustness of the oscillation interpretation against departures from the Standard Solar Model and the possible existence of non-standard neutrino physics. Furthermore, we give the best-fit values and allowed ranges of the three flavoured oscillation parameters from the current world's global neutrino data sample and discuss in detail the status of the small parameters $m_{sol}^2 = m_{atm}^2$ as well as $\sin^2 \theta_{13}$, which characterize the strength of CP violating effects in neutrino oscillations. We also update the degree of rejection of four-neutrino interpretations of the LSND anomaly in view of the most recent developments.

PACS numbers: 26.65.+t, 13.15.+g, 14.60.Pq, 95.55.Vj

Keywords: Neutrino mass and mixing; solar and atmospheric neutrinos; reactor and accelerator neutrinos

^xElectronic address: maltoni@ific.uv.es

^yElectronic address: schwetz@ph.tum.de

^zElectronic address: marian@ific.uv.es

^xElectronic address: valle@ific.uv.es

Contents

I. Introduction	3
II. Leading oscillations with m_{atm}^2	4
A. Atmospheric neutrino oscillations	4
B. The K2K accelerator experiment	5
C. Atmospheric and K2K combined	7
D. Robustness of oscillation interpretation: atmospheric neutrinos	7
III. Leading oscillations with m_{sol}^2	10
A. Solar neutrino oscillations	10
B. The KamLAND reactor neutrino experiment	12
C. Solar and KamLAND combined	15
D. Robustness of oscillation interpretation: solar neutrinos	15
1. Beyond the Standard Solar Model	15
2. Beyond solar neutrino oscillations: Spin Flavour Precession	18
3. Beyond SM neutrino cross sections: Constraining neutrino magnetic moments	19
IV. Three-flavour neutrino oscillations	21
A. Global three-neutrino analysis	21
B. The small parameters $m_{sol}^2 = m_{atm}^2$ and $_{13}$	23
V. Four-neutrino oscillations and LSND	27
A. A common parametrization for four-neutrino schemes	27
B. (2+2): ruled out by solar and atmospheric data	28
C. (3+1): strongly disfavoured by SBL data	30
D. Comparing (3+1), (2+2) and (3+0) hypotheses	31
VI. Summary and conclusions	33
Acknowledgments	34
References	34

I. INTRODUCTION

The discovery of neutrino masses by the combination of a variety of data from solar [1, 2, 3, 4, 5, 6, 7, 8, 9, 10], atmospheric [11, 12, 13], reactor [14] and accelerator [15] neutrino experiments was the major recent achievement in astroparticle, high energy, and nuclear physics, which culminates a heroic effort dating back to about four decades. This has now firmly established the incompleteness of the Standard Model of electroweak interactions, expected on theoretical grounds since long ago [16, 17, 18, 19, 20]. The determination of neutrino oscillation parameters is now a flourishing industry [21] which has finally entered the high precision age, with many experiments underway and a new generation coming. Apart from a careful understanding of solar and atmospheric neutrino fluxes, nuclear physics, neutrino cross sections and experimental response functions, the interpretation of the data relies heavily on the proper description of neutrino propagation properties both in the Sun and the Earth, including the so-called matter effects [22, 23].

The avalanche of data in a field where these have been traditionally so scarce, given the feebleness of neutrino interactions, has prompted a rush of phenomenological papers on the interpretation of neutrino data. A number of reviews are already in the market [24, 25, 26, 27]. Here we revisit the latest global analysis of neutrino oscillation parameters presented in Ref. [28] in view of the most recent solar [29] and atmospheric [30] neutrino flux calculations.

This paper is organized as follows. In Sec. II we briefly discuss the analysis of the atmospheric neutrino data including the state-of-the-art three-dimensional calculation of the atmospheric neutrino flux given in Ref. [30]. In order to obtain the allowed ranges for the oscillation parameters m_{atm}^2 and δ_{atm} we combine the atmospheric neutrino data from the Super-K experiment with the accelerator data from the K2K experiment, which provides the first independent confirmation of the oscillation evidence from atmospheric neutrinos. We give also a short description of robustness of the atmospheric data with respect to non-standard neutrino interactions in Sec. IID.

In Sec. III we briefly describe the solar neutrino experiments and the KamLAND reactor neutrino experiment, and discuss the two-neutrino interpretation of the data described by m_{sol}^2 and δ_{sol} . We comment on the implications of the recent update of the Standard Solar Model (SSM) neutrino fluxes from Ref. [29]. Furthermore, in Sec. IID we discuss the robustness of the oscillation interpretation of solar neutrino data when going beyond the SSM framework or invoking non-standard neutrino properties. As examples we consider the effects of solar radiative-zone density fluctuations, convective-zone magnetic fields and the prospects of probing electromagnetic neutrino properties with current and future experiments.

After discussing the dominant oscillations in the two-flavour approximation in Secs. II and III we devote Sec. IV to the global three-neutrino analysis of the data, combining all

current neutrino oscillation data except LSND. In addition to presenting the best t values and allowed ranges for the oscillation parameters, we analyse the status of the three-flavour parameters $m_{sol}^2 = m_{atm}^2$ and θ_{13} . In Sec. V we give an update of the status of attempts to account for the LSND data in terms of four-neutrino oscillations. Finally we conclude and summarize our results in Sec. VI.

II. LEAD IN G OSCILLATIONS WITH m_{atm}^2

A. Atm ospheric neutrino oscillations

In 1998 the Super-K experiment obtained evidence for neutrino oscillations [11] from the observation of the zenith angle dependence of their $\bar{\nu}$ -like atmospheric neutrino data. This effect has been confirmed also by other atmospheric neutrino experiments, see e.g. Refs. [12, 13]. Recently, Super-K has reported a dip in the $L=E$ distribution of the atmospheric survival probability [31], which provides a clear signature for neutrino oscillations.

In our atmospheric neutrino analysis we include the most recent charged-current atmospheric neutrino data from Super-K [32], including the e -like and $\bar{\nu}$ -like data samples of sub- and multi-GeV contained events (each grouped into 10 bins in zenith angle), as well as the stopping (5 angular bins) and through-going (10 angular bins) up-going muon data events. As previously, we do not use the information on appearance, multi-ring and neutral-current events since an efficient Monte-Carlo simulation of these data would require a more detailed knowledge of the Super-K experiment, and in particular of the way the neutral-current signal is extracted from the data. For details of our analysis see Refs. [33, 34] and references therein. With respect to our previous atmospheric neutrino analysis [28] we have now taken into account the new three-dimensional atmospheric neutrino fluxes given in Ref. [30]. Furthermore, we have updated our statistical analysis following closely Ref. [35], taking special care of systematical errors, like uncertainties in the neutrino fluxes and detection cross sections. Details on the χ^2 analysis can also be found in Ref. [36]. With these updates our results are in excellent agreement with the ones of the Super-K Kamiokande collaboration [32].

In Fig. 1 we show the results of our analysis of atmospheric data in the framework of two-flavour neutrino oscillations. The regions delimited by the hollow contours correspond to the allowed regions for the oscillation parameters $\sin^2 \theta_{atm}$ and m_{atm}^2 . The current best fit point occurs at

$$\sin^2 \theta_{atm} = 0.50; \quad m_{atm}^2 = 2.0 \times 10^{-3} \text{ eV}^2 \quad (\text{ATM data}): \quad (1)$$

The main difference to the results of Ref. [28] are the relatively lower values of m_{atm}^2

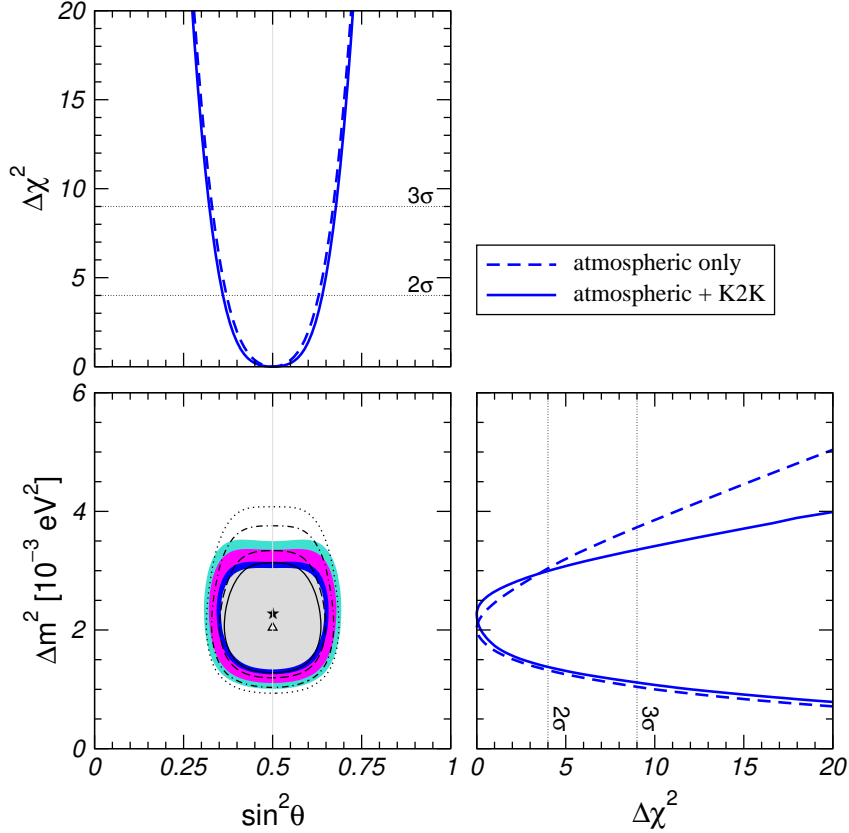


Figure 1: Allowed $(\sin^2 \theta_{\text{atm}}, m_{\text{atm}}^2)$ regions at 90%, 95%, 99%, and 3 C.L. for 2 d.o.f. The regions delimited by the lines correspond to atmospheric data only, while for the colored regions also K2K data are added. The best fit point of atmospheric (atmospheric + K2K) data is marked by a triangle (star). Also shown is the χ^2 as a function of $\sin^2 \theta_{\text{atm}}$ and m_{atm}^2 , minimized with respect to the undisplayed parameter.

implied by the use of the new three-dimensional atmospheric neutrino fluxes reported in Ref. [30] instead of the one-dimensional Bartol fluxes [37] used previously.

B. The K2K accelerator experiment

The KEK to Kamioka (K2K) long-baseline neutrino oscillation experiment [15] probes the disappearance oscillation channel in the same region of m^2 as explored by atmospheric neutrinos. The neutrino beam is produced by a 12 GeV proton beam from the KEK proton synchrotron, and consists of 98% muon neutrinos with a mean energy of 1.3 GeV. The beam is controlled by a near detector 300 m away from the proton target. Information on neutrino oscillations is obtained by the comparison of this near detector data with the content of the beam observed by the Super-Kamiokande detector at a distance of 250 km. In the period

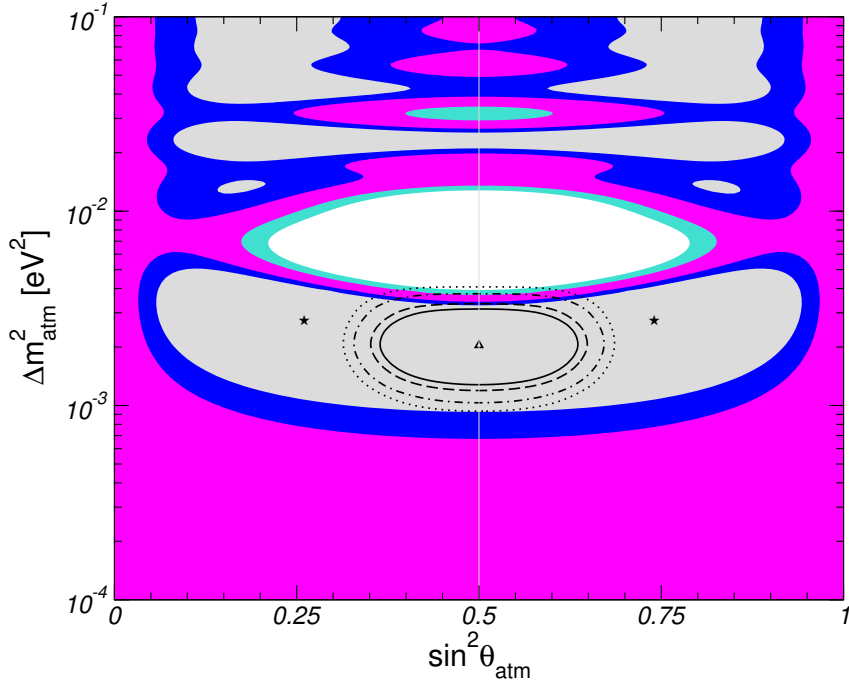


Figure 2: Allowed K2K regions in the $(\sin^2 \theta_{\text{atm}}, m_{\text{atm}}^2)$ plane at 90%, 95%, 99%, and 3 C.L. for 2 d.o.f. The hollow lines delimit the region determined from the atmospheric neutrino data only.

from June 1999 to July 2001 (4.8×10^9 protons on target) 56 events have been observed in Super-K, whereas $80.1^{+6.2}_{-5.4}$ have been expected in the case of no oscillations [15]. This gives a clear evidence for disappearance: the probability that the observed flux at Super-K is explained by a statistical fluctuation without neutrino oscillations is less than 1% [15].

In our re-analysis of K2K data we use the energy spectrum of the so-called single-ring muon event sample, which consists of 29 events. This data sample contains mainly muon events from the quasi-elastic scattering $\nu + p \rightarrow \nu + n$, and hence, the reconstructed energy is closely related to the true neutrino energy¹. For the analysis of these spectral data we follow the method described in Ref. [36]. The data are divided into 6 bins in reconstructed neutrino energy and we include systematical errors in the χ^2 analysis as given in Ref. [36]. The allowed regions for the oscillation parameters from K2K data are shown in Fig. 2 in comparison to the ones from atmospheric neutrino data. This figure illustrates that the neutrino mass-squared difference indicated by the disappearance observed in K2K is in perfect agreement with atmospheric neutrino oscillations. Hence, K2K data provides the first confirmation of oscillations with m_{atm}^2 from a man-made neutrino source. K2K gives a rather weak constraint on the mixing angle due to low statistics in the current data sample.

¹ We cannot use the full K2K data sample of 56 events, since not enough information is available to analyze these data outside the K2K collaboration.

C . A tm ospheric and K 2K combined

In Fig. 1 the allowed regions in the $(\sin^2_{\text{atm}}, m_{\text{atm}}^2)$ plane from the combined analysis of K 2K and Super-K atm ospheric neutrino data are shown as shaded regions. As expected from Fig. 2 we find that the first 29 events from K 2K included here start already to constrain the upper region of m_{atm}^2 , whereas the determination of the mixing angle is completely dominated by the atm ospheric data. From the projections of the χ^2 onto the m_{atm}^2 and \sin^2_{atm} axes shown in Fig. 1 we find the best fit point

$$\sin^2_{\text{atm}} = 0.5; \quad m_{\text{atm}}^2 = 2.3 \times 10^3 \text{ eV}^2 \quad (\text{ATM} + \text{K 2K data}) \quad (2)$$

with the corresponding allowed ranges at 3 (5) for 1 d.o.f.:

$$\begin{aligned} 0.32 \text{ (0.26)} & \quad \sin^2_{\text{atm}} & 0.68 \text{ (0.74)}; \\ 1.1 \text{ (0.69)} & \quad 10^3 \text{ eV}^2 & m_{\text{atm}}^2 & 3.4 \text{ (4.3)} \quad 10^3 \text{ eV}^2; \end{aligned} \quad (3)$$

Note that despite the downward shift of the atm ospheric mass splitting implied by the new neutrino fluxes from Ref. [30] our new quoted value for m_{atm}^2 in Eq. (2) is statistically compatible both with our previous result [28] and the value obtained by the new Super-K L=E analysis [31].

D . Robustness of oscillation interpretation: atm ospheric neutrinos

We now turn to the issue of the robustness of the oscillation interpretation of the atm ospheric neutrino data. Non-standard physics may in principle affect atm ospheric neutrino fluxes, as well as neutrino propagation and detection cross sections [24]. Apart from the issue of their theoretical viability [38] neutrino decays have been considered since long ago [39]. Non-standard interactions arising from the SU(2) \times U(1) charged and neutral currents [8] or from new particles [40, 41, 42, 43, 44, 45, 46], as well as quantum mechanical decoherence [36] might also affect atm ospheric neutrino results. Although strongly rejected by recent atm ospheric data as the dominant mechanism [31, 36, 47], non-standard phenomena might still be present at a sub-leading level in addition to oscillations and, to this extent, have some impact on the determination of the oscillation parameters.

In the following we illustrate the stability of the measurement of m_{atm}^2 and \sin^2_{atm} by assuming the presence of non-standard interactions of the neutrinos with earth matter. New neutrino interactions beyond the Standard Model are a natural feature in most neutrino mass models [48] and can be of two types: flavour-changing (FC) and non-universal (NU). These interactions (called NSI for short) may be schematically represented as effective

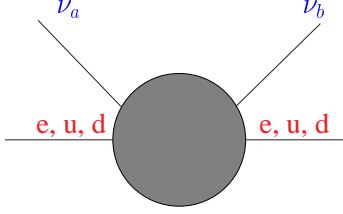


Figure 3: Effective flavor-changing NSI operator.

dimension-6 terms of the type " G_F ", as illustrated in Fig. 3, where " G " specifies their sub-weak strength. Such interactions may arise from a nontrivial structure of charged and neutral current weak interactions characterized by a non-unitary lepton mixing matrix [18]. These gauge-induced NSI may lead to flavor and CP violation, even with massless or degenerate neutrinos [42, 44, 45, 46]. Alternatively, such non-standard neutrino interactions may also arise in models where neutrino masses are "calculable" from radiative corrections [40, 41] and in some supersymmetric models with broken R parity [49]. Finally, in supersymmetric unified models, the strength of non-standard neutrino interactions may be a calculable renormalization effect [43].

The impact of non-standard neutrino interactions on atmospheric neutrinos was considered in Ref. [47] treating the NSI strengths as free phenomenological parameters. This analysis takes into account both the effect of $\nu_e \rightarrow \nu_e$ oscillations (OSC) as well as the existence of non-standard neutrino-matter interactions (NSI) in this channel. In addition to the standard term in the Hamiltonian describing oscillations an term H_{NSI} is introduced, accounting for an effective potential induced by the NSI with earth matter:

$$H_{\text{NSI}} = \frac{p_-}{2G_F N_f} \begin{matrix} 0 & " \\ " & 0 \end{matrix} : \quad (4)$$

Here $+$ ($-$) holds for neutrinos (anti-neutrinos) and " $"$ " and " $"^0$ " parametrize the NSI: $\frac{p_-}{2G_F N_f}$ is the forward scattering amplitude for the FC process $\nu_e + f \rightarrow \nu_e + f$ and $\frac{p_-}{2G_F N_f}$ represents the difference between $\nu_e + f$ and $\bar{\nu}_e + f$ elastic forward scattering. The quantity N_f is the number density of the fermion f along the neutrino path. For definiteness we take for f the down-type quark.

In Fig. 4 we show the results of a fit to atmospheric neutrino data for the four parameters m_{atm}^2 , $\sin^2 2_{\text{atm}}$, " $"$ ", and " $"^0$ ".² In the left panels the pure oscillation case (" $" = " $"^0 = 0$ ") is compared to the case where also some NSI are allowed. We find that the χ^2 improves slightly (2.4 units) in the presence of NSI, but the determination of the oscillation parameters is$

² Here we assume that the parameter " $"$ " is real; for the more general case of complex " $"$ ", see Ref. [50].

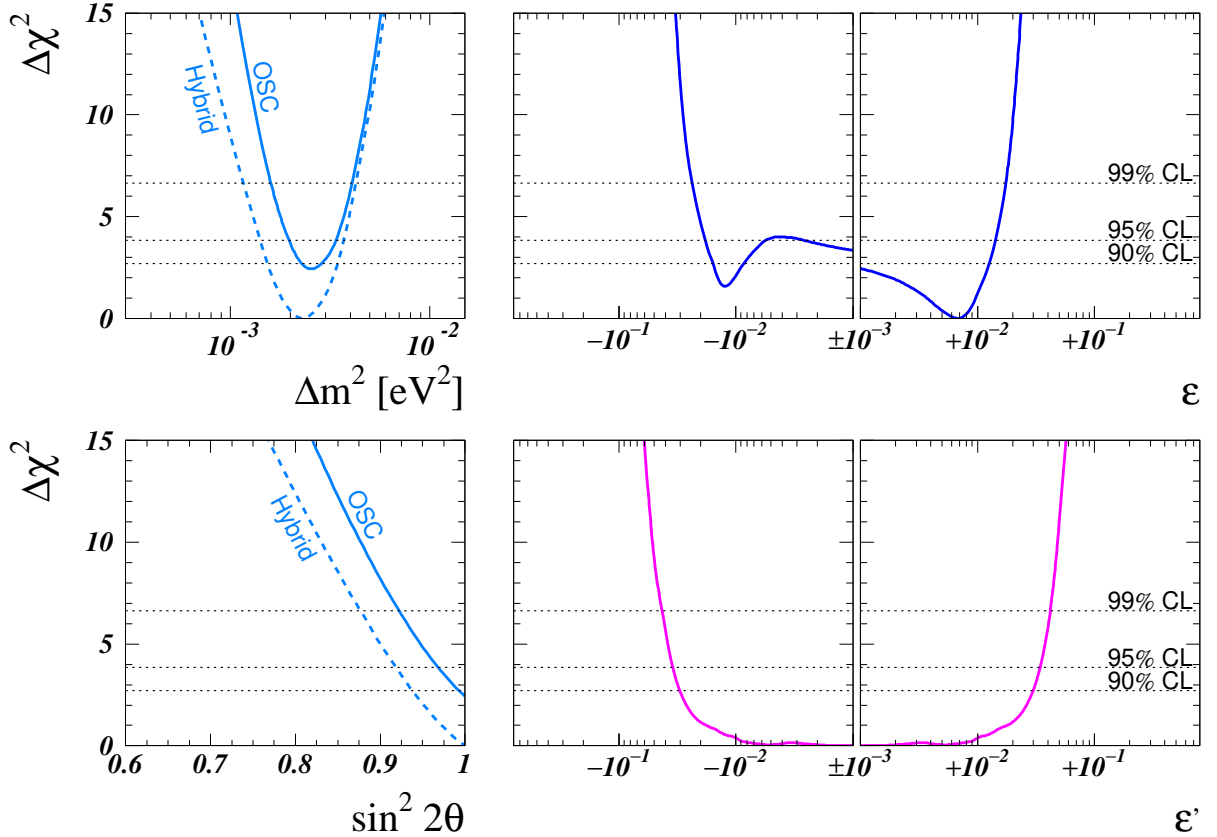


Figure 4: Fit of oscillations and NSI to atmospheric neutrino data [47]. We show the behaviour of the χ^2 as a function of the four parameters m_{atm}^2 (upper left), $\sin^2 2\theta_{\text{atm}}$ (lower left), the FC parameter ϵ (upper right), and the NU parameter ϵ^0 (lower right). In each panel the χ^2 is minimized with respect to the three undisplayed parameters. In the left panels we show also the pure oscillation case (OSC), with ϵ and ϵ^0 set to zero.

practically unaffected. This is an important result, since it shows that the allowed ranges derived for m_{atm}^2 and $\sin^2 2\theta_{\text{atm}}$ are rather stable with respect to non-standard physics³. In turn, the high preference of the data for oscillations allows to set strong bounds on NSI. From the right panels of Fig. 4 we deduce the bounds at 3

$$0.03 \quad \epsilon \quad 0.02; \quad \epsilon^0 \quad 0.05: \quad (5)$$

Before closing we stress that, apart from its intrinsic theoretical importance, the study of non-standard neutrino interactions has an astrophysical interest, as these can affect the

³ Note that the analysis of Ref. [47] is based on the neutrino fluxes of Ref. [37], and in addition to the Super-K data described in Sec. II A also the up-going muon data from the MACRO experiment [12] is used. This explains the slight difference between the best fit values of m_{atm}^2 from Fig. 4 for the pure oscillation case and Eq. (1).

propagation of neutrinos in a variety of astrophysical environments, such as supernovae [51, 52] and pulsars [53]. They could lead to "deep-inside" neutrino conversions, in addition to those expected from conventional neutrino oscillations.

III. LEAD ING OSCILLATIONS WITH m_{sol}^2

A. Solar neutrino oscillations

In this section we consider oscillations of solar neutrinos in the two-flavour framework. A detailed discussion of experimental and theoretical aspects of solar neutrino physics can be found in other contributions to this volume [54, 55]. Therefore, we focus in the following on the determination of the oscillation parameters from the fit to solar neutrino data. In our analysis we take into account the rates of the chlorine experiment at the Homestake mine [1, 2] (2.56 \pm 0.16 \pm 0.16 SNU), the most up-to-date results [56] of the gallium experiments SAGE [3, 57] ($69.1 \pm 4.3 \pm 3.8$ SNU) and GALLEX/GNO [4, 5, 6] ($69.3 \pm 4.1 \pm 3.6$ SNU), as well as the 1496-day Super-Kamiokande data sample [7] in the form of 44 bins (8 energy bins, 6 of which are further divided into 7 zenith angle bins). From the SNO experiment we include the most recent data from the salt phase [10] in the form of the neutral current (NC), charged current (CC) and elastic scattering (ES) fluxes, as well as the 2002 spectral day/night data [8, 9] (17 energy bins for each day and night period).

The analysis methods used here are similar to the ones described in Refs. [28, 34] and references therein, including the use of the so-called pull approach for the χ^2 calculation, as described in Ref. [58]. In this method all systematic uncertainties are included by introducing new parameters in the fit and adding a penalty function to the χ^2 . For example, for each of the eight solar neutrino fluxes a parameter is introduced, and the predictions from the Standard Solar Model including the correlated errors are taken into account by means of a penalty function. The method described in Ref. [58] is extended in two respects: First, it is generalized to the case of correlated statistical errors [59] as necessary to treat the SNO (salt) data. Second, we do not consider the χ^2 only up to first order in the pulls, but instead each pull parameter is treated exactly to all orders. This is particularly interesting in the case of the solar ${}^8\text{B}$ flux. In our approach it is possible to include the SSM prediction for this flux as well as the SNO NC measurement on the same footing, without pre-selecting a particular value, as implied by expanding around the predicted value. In this way the fit itself can choose the best compromise between the SNO NC data and the SSM prediction.

In Fig. 5 we compare the allowed regions for the oscillation parameters using the solar neutrino fluxes given in the BP00 SSM [60] and the recent update (BP04) presented in Ref. [29]. One finds that the change in the flux predictions has a negligible impact on

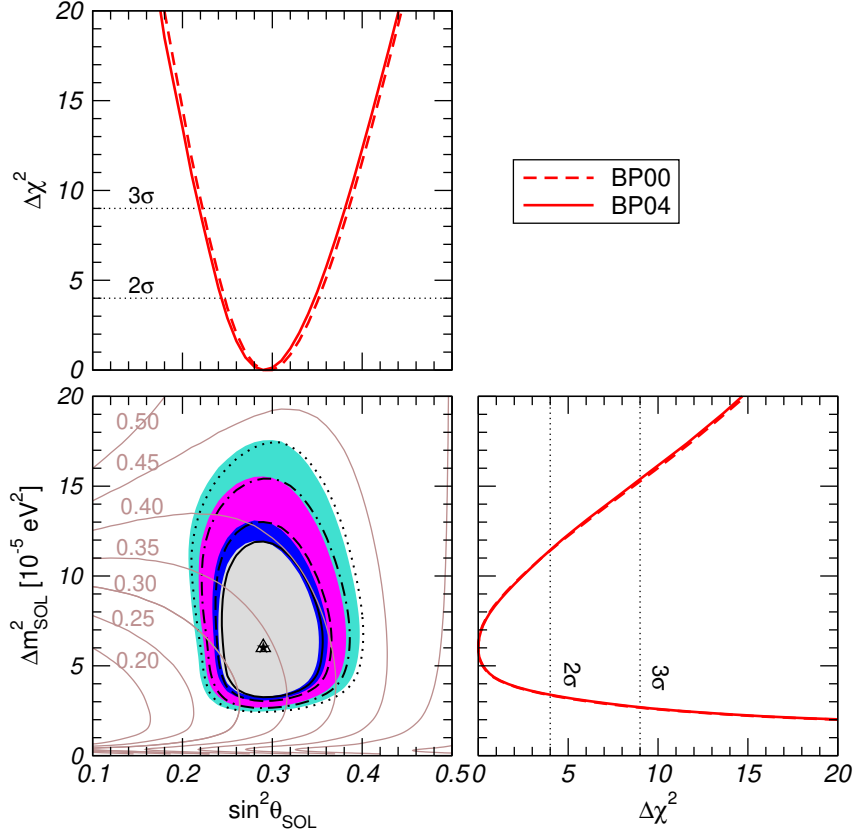


Figure 5: Allowed regions from all solar neutrino data at 90%, 95%, 99%, and 3 C.L. for 2 d.o.f. in the plane of $\sin^2\theta_{\text{SOL}}$ and Δm_{SOL}^2 . The regions delimited by the curves correspond to the BP00 SSM [60], whereas for the colored regions the BP04 SSM [29] has been used. Also shown is $\Delta\chi^2$ as a function of $\sin^2\theta_{\text{SOL}}$ and Δm_{SOL}^2 , minimized with respect to the undisplayed parameter. The labeled contours denote constant CC/NC ratio in the SNO experiment.

the allowed regions. This illustrates that thanks to the good experimental accuracy the determination of the oscillation parameters is rather robust with respect to changes in the SSM. The current best t values for solar neutrino oscillation parameters are

$$\sin^2\theta_{\text{SOL}} = 0.29; \quad \Delta m_{\text{SOL}}^2 = 6.0 \times 10^{-5} \text{ eV}^2 \quad (\text{solar data, BP04}); \quad (6)$$

Also the rejection against maximal solar mixing is 5.6, the same as found previously [28] using the BP00 solar model. This is the significance at which bimaximal models of neutrino mass, such as the CP conserving version of the neutrino unitary model given in Ref. [61], are ruled out. Despite the fact that the BP04 model does not imply any significant change in the solar neutrino parameters, we will use it in our subsequent discussion of solar neutrino results.

B . The KamLAND reactor neutrino experiment

The KamLAND experiment [14] is a reactor neutrino experiment with its detector located at the Kamiookande site. Most of the ν_e incident at KamLAND comes from nuclear plants at distances of 80 – 350 km from the detector, making the average baseline of about 180 kilometers, long enough to provide a sensitive probe of the LMA solution of the solar neutrino problem. The KamLAND collaboration has for the first time measured the disappearance of neutrinos traveling to a detector from a power reactor. They observe a strong evidence for the disappearance of neutrinos during their flight over such distances, giving the first terrestrial confirmation of the solar neutrino anomaly and also establishing the oscillation hypothesis with man-produced neutrinos.

In KamLAND the reactor anti-neutrinos are observed by the process $e^- + p \rightarrow e^+ + n$, where the delayed coincidence of the prompt energy from the positron and a characteristic gamma from the neutron capture allows an efficient reduction of backgrounds. The neutrino energy is related to the prompt energy by $E_\nu = E_{\text{pr}} + m_e$, where m_e is the neutron-proton mass difference and m_e is the positron mass. The current KamLAND data sample consists of 86 anti-neutrino events in the full energy range. In the lower part of the spectrum there is a relevant contribution from geo-neutrino events to the signal (see, e.g., Refs. [62, 63]). To avoid large uncertainties associated with the geo-neutrino flux an energy cut at 2.6 MeV prompt energy is applied for the oscillation analysis, and $N_{\text{obs}} = 54$ anti-neutrino events remain in the sample. This number has to be compared with $N_{\text{pred}} = 86.8 \pm 5.6$ reactor neutrino events predicted for no oscillations and $N_{\text{BG}} = 0.95 \pm 0.99$ background events, which leads to

$$\frac{N_{\text{obs}}}{N_{\text{pred}}} = 0.611 \pm 0.085 \text{ (stat)} \pm 0.041 \text{ (syst)} : \quad (7)$$

The probability that the KamLAND result is consistent with the no-disappearance hypothesis is less than 0.05% [14].

In order to extract most of the information from the spectral data we adopt the event-based likelihood analysis presented in Ref. [64]. For a given set of neutrino oscillation parameters $\sin^2 \theta_{\text{sol}}$ and m_{sol}^2 the predicted spectrum $f(E_{\text{pr}}; \sin^2 \theta_{\text{sol}}; m_{\text{sol}}^2)$ of events with prompt energy E_{pr} can be calculated by a convolution of the neutrino flux, the oscillation survival probability, the detection cross section, and the energy resolution function. The contributions of the 16 power plants have to be properly weighted according to the distances from the detector and the individual thermal reactor powers. Details of our KamLAND simulation can be found in Refs. [64, 65]. The magnitudes of the relevant baselines and neutrino energies in KamLAND imply that it is an excellent approximation to use the vacuum neutrino oscillation probability. For the statistical analysis we apply a standard

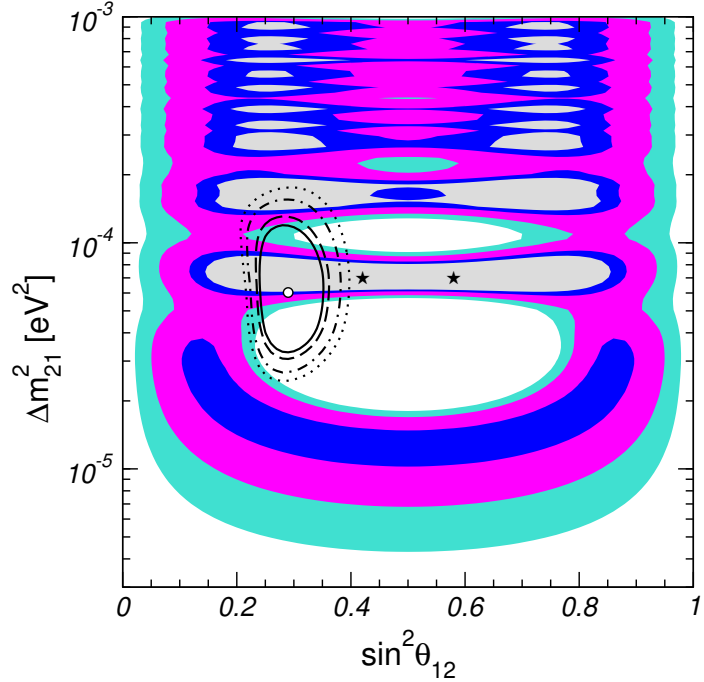


Figure 6: Allowed regions from KamLAND data at 90%, 95%, 99%, and 3 C.L. for 2 d.o.f.. The regions delimited by the lines correspond to solar data. The KamLAND best fit points are marked with a star, the solar best fit point with a dot.

likelihood method, where the total likelihood function is given by $L_{\text{tot}} = L_{\text{rate}} \cdot L_{\text{shape}}$. Here L_{rate} takes into account the information from the total number of observed events, and the spectral shape information is contained in L_{shape} . The latter is obtained from the individual prompt energies of the 54 events observed above the geo-neutrino cut, which can be found in Tab. 1 of Ref. [64]. The results of the statistical analysis performed in this way are in excellent agreement with the original KamLAND analysis from Ref. [14].

By maximizing the likelihood function L_{tot} we obtain the best fit parameters

$$m_{\text{sol}}^2 = 7.05 \cdot 10^{-5} \text{ eV}^2; \quad \sin^2 2 \theta_{\text{sol}} = 0.98 \quad (\text{KamLAND data}); \quad (8)$$

The KamLAND allowed regions for $\sin^2 \theta_{\text{sol}}$ and m_{sol}^2 obtained from contours of constant L_{tot} are shown in Fig. 6 in comparison to the regions from solar data. One observes beautiful agreement between KamLAND data and the region implied by the LMA solution to the solar neutrino problem, which in this way has been singled out as the only viable one. Before this experiment we had a very complex pattern of alternative oscillation solutions like LOW, SMA, or VAC, see e.g., Refs. [33, 34]. A lot of these are completely ruled out by the KamLAND data. From this point of view the KamLAND experiment has played a fundamental role in the resolution of the solar neutrino problem. However, one also observes from Fig. 6 that KamLAND data on its own allows still a rather large range for the oscillation parameters.

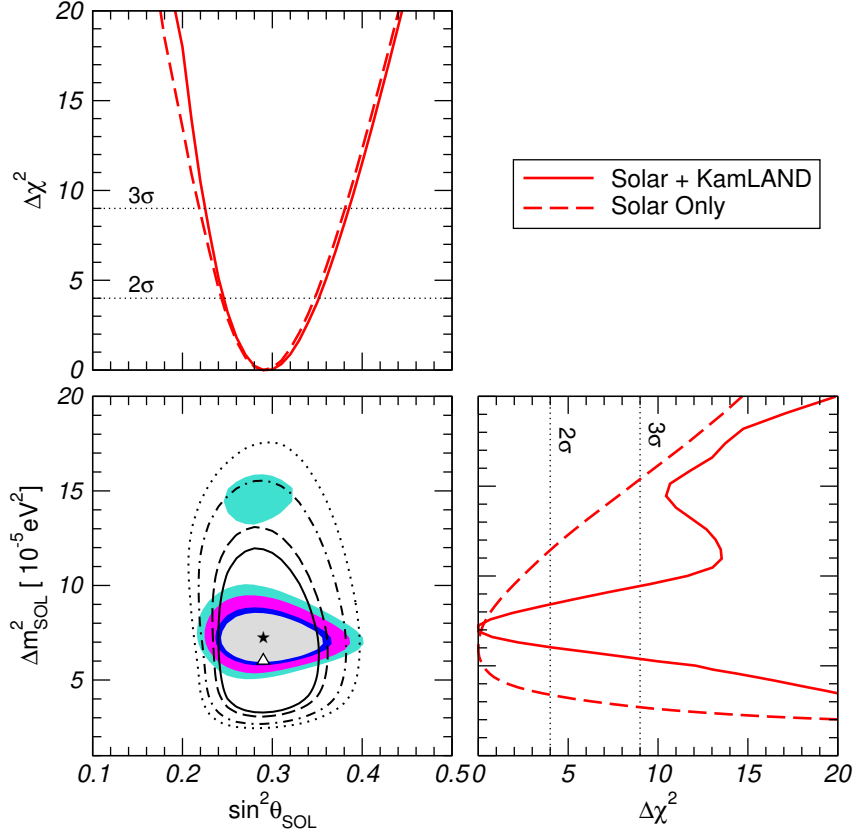


Figure 7: Allowed regions from combined solar and KamLAND data at 90%, 95%, 99%, and 3 C.L. for 2 d.o.f.. The regions shown with lines correspond to solar data only from Fig. 5.

In particular, high values of $m_{\text{sol}}^2 \gtrsim 3 \times 10^4 \text{ eV}^2$ in the averaging regime are allowed at 90% C.L.. This implies that the current KamLAND data sample is consistent with an energy independent suppression of the neutrino flux. Although there are some hints for spectral distortion in the data (the χ^2 improves roughly by 4 units if oscillations are allowed with respect to the energy independent suppression) the oscillatory signal has not yet been established with high significance. The neutrino community is eagerly awaiting the release of new data from KamLAND, which might finally accomplish this task.

Let us add that an explicit Monte Carlo simulation of the KamLAND experiment [64] has shown that the allowed regions obtained as described here are a good approximation to confidence regions with exact coverage, despite the fact that the current data sample is rather small.

C. Solar and KamLAND combined

Under the fundamental assumption of CPT invariance we can directly compare the information obtained from solar neutrino experiments and the KamLAND reactor experiment. In Fig. 7 we show the allowed regions from the combined solar and KamLAND data. The current best fit point of the global analysis occurs at

$$\sin^2 \theta_{\text{sol}} = 0.29; \quad m_{\text{sol}}^2 = 7.2 \times 10^5 \text{ eV}^2 \quad (\text{SOL BP04+KAM data}); \quad (9)$$

From the projections of the χ^2 onto the m_{sol}^2 and $\sin^2 \theta_{\text{sol}}$ axes also shown in Fig. 7 we find the following allowed ranges at 3 (5) for 1 d.o.f.:

$$\begin{aligned} 0.23 \text{ (0.17)} & \quad \sin^2 \theta_{\text{sol}} & 0.39 \text{ (0.47)}; \\ 5.4 \text{ (2.1)} & \quad 10^5 \text{ eV}^2 & m_{\text{sol}}^2 & 9.4 \text{ (28)} & \quad 10^5 \text{ eV}^2; \end{aligned} \quad (10)$$

As expected from Fig. 6 the determination of the mixing angle is completely dominated by the solar neutrino data, whereas KamLAND significantly reduces the allowed range for m_{sol}^2 . We note that the use of the BP04 fluxes has not changed significantly the allowed regions. The so-called high-LMA region still appears at the 3 level. The local χ^2 minimum corresponding to high-LMA has a $\chi^2 = 10.5$ with respect to the global minimum, which corresponds to an exclusion at about 2.8 for 2 d.o.f.. Notice also that the day/night data are treated as previously [28, 34]. An improved analysis of the day/night asymmetry data along the lines followed by the SuperKamiokande collaboration in Ref. [66] would lead to a more pronounced rejection of the high m_{sol}^2 region. Currently not enough information is available to reproduce this result outside the SuperKamiokande collaboration.

D. Robustness of oscillation interpretation: solar neutrinos

The oscillation interpretation of solar neutrino data depends both on astrophysical input (the model of the Sun) as well as on the physics characterizing both the propagation as well as neutrino interaction properties. Either may differ from the Standard Solar Model and Standard Electroweak Model expectations. How robust is the oscillation interpretation of solar neutrino data in view of this?

1. Beyond the Standard Solar Model

In the following we will briefly discuss consequences of departures from the Standard Solar Model. As a case study we consider the possibility of solar density fluctuations. Even though

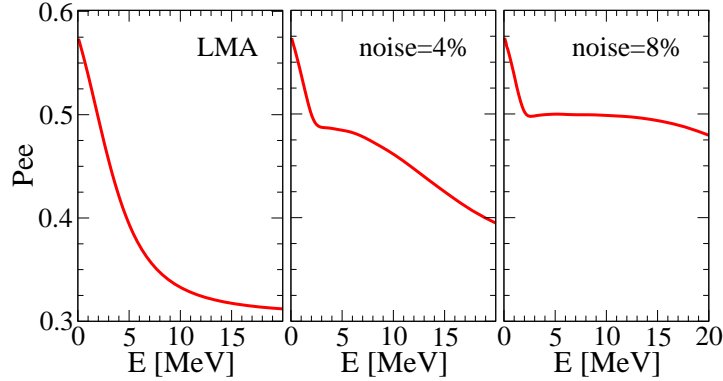


Figure 8: Effect of random matter density fluctuations with a correlation length of $L_0 = 100$ km on the electron-neutrino survival probability for LMA oscillations.

this possibility was suggested in a number of papers [67, 68, 69] it has been traditionally neglected for several reasons. First, helioseismic measurements constrain deviations of solar properties from Standard Solar Model predictions at better than the percent level. Second, preliminary studies of the implications for neutrino oscillations of radiative-zone helioseismic waves [69] indicated that they were unlikely to have observable effects. Third, no other known sources of fluctuations seemed to have the properties required to influence neutrino oscillations.

Recently all of these points have been re-examined, with the result that the presence of solar fluctuations appears more likely than previously thought. First, direct helioseismic bounds turn out to be insensitive to fluctuations whose size is as small as those to which neutrinos are sensitive [70, 71] typically several hundreds of km. Second, recent studies have shown how such solar density fluctuations can arise near the solar equatorial plane in the presence of magnetic fields deep within the solar radiative zone due to a resonance between Alfvén waves and helioseismic modes [72].

It has been shown in Ref. [73] that such density fluctuations can affect neutrino propagation in an important way. The effect of random matter density fluctuations on the electron-neutrino survival probability for LMA oscillations has been shown to be sizeable if the correlation length L_0 (we take $L_0 = 100$ km) is comparable to the neutrino oscillation length in the Sun. This is illustrated in Fig. 8. The fluctuation's amplitude at the position of neutrino resonance is zero in the left panel, and is $\sigma = 4\%$ and $\sigma = 8\%$ in the middle and right panels, respectively. The corresponding solar neutrino oscillation parameters obtained in our global fit are shown in Fig. 9. One sees that the presence of solar noise has some impact on the allowed regions from solar data alone. Once KamLAND is taken into account the determination of m_{sol}^2 and δ_{sol} is stable at 95% CL, however, a new allowed region appears for $m_{\text{sol}}^2 \approx 2 \times 10^5$ eV² at the 99% CL..

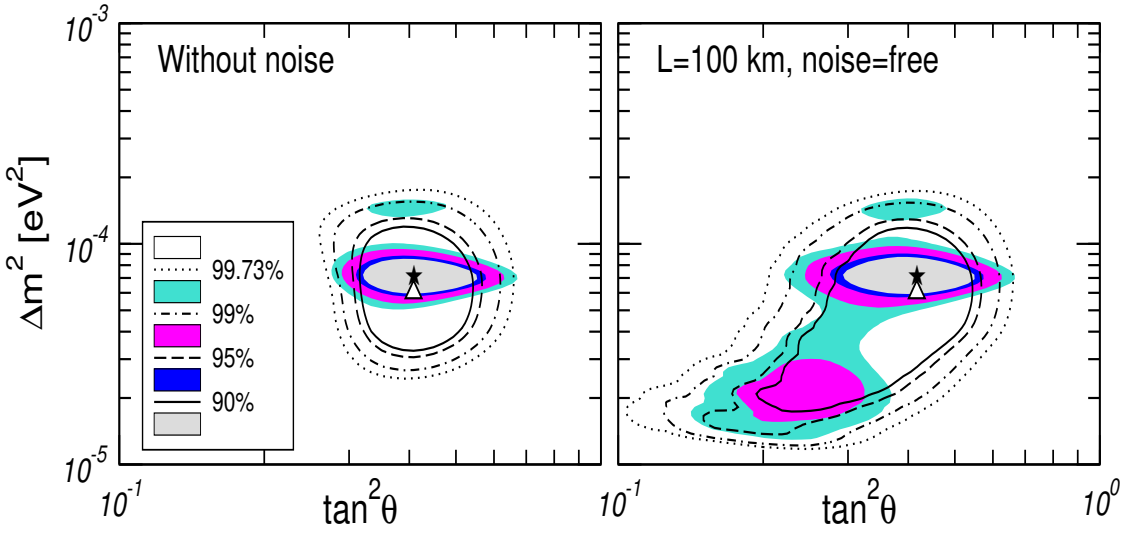


Figure 9: Solar neutrino oscillation parameters with no noise (left panel), and with an arbitrary noise amplitude and a correlation length $L_0 = 100$ km (right panel). The coloured regions are obtained using the KamLAND data, while the lines refer to C.L. contours without KamLAND.

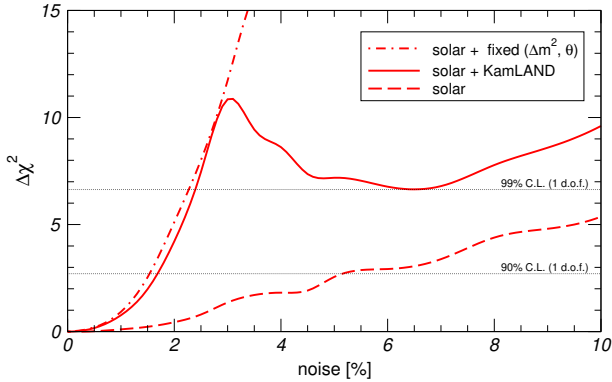


Figure 10: Bounds on random matter density fluctuations for a correlation length of $L_0 = 100$ km from solar neutrino data, solar + KamLAND data, and solar data for oscillation parameters fixed at the best fit point.

Conversely, as shown in Ref. [74], the quality of current solar neutrino measurements after the SNO+ salt results is sufficiently good as to place important constraints on fluctuations in the solar medium deep within the solar radiative zone. In other words, neutrinos may be used as an astrophysical probe of the solar interior, beyond the framework of the Standard Solar Model. As illustrated in Fig. 10 density fluctuations are strongly constrained if the correlation length lies in the range of several hundred km. Comparing the curves for free and fixed oscillation parameters one notes that the bounds on fluctuations will become more stable, when the accuracy on m_{sol}^2 and θ_{sol} gets improved by future neutrino experiments,

e.g., by future KamLAND data. Because oscillations are sensitive to correlation lengths which are so short, such solar neutrino results will complement the constraints that come from helioseismology.

2. Beyond solar neutrino oscillations: Spin Flavour Precession

In extensions of the Standard Model (SM) neutrino masses are in general accompanied also by non-standard interactions and/or electromagnetic properties. In the minimal extension of the Standard Model with Dirac neutrino masses one expects very tiny neutrino magnetic moments (MMs) [75], well below current experimental sensitivities. However, the theoretically preferred case of Majorana neutrinos leads to potentially larger transition magnetic moments closer to the present sensitivities. The possible existence of non-trivial electromagnetic neutrino properties can affect (i) neutrino propagation properties in the Sun beyond the oscillation mechanism, due to the possible presence of solar magnetic fields, and (ii) the neutrino cross sections inside the detectors.

The most general form of the electromagnetic current of massive (Majorana) neutrinos has been given in Ref. [76]. The magnetic piece is characterized by a 3×3 complex antisymmetric matrix, the so-called Majorana transition moment (TM) matrix, that contains MMs as well as electric dipole moments of the neutrinos. Their existence would affect neutrino propagation inside the solar convective zone due to a spin-flavor precession (SFP) effect [76, 77, 78]. This in general depends on the assumed magnetic field profile. In order to quantify the extent with which the oscillation regions can be altered by the sub-leading spin-flavor precession effect, a 2 analysis was performed in Ref. [79] taking into account the global solar + KamLAND disappearance data. We assumed that neutrino conversions are driven mainly by LMA oscillations, and used the same self-consistent [80] convective zone solar magnetic field profile employed in Ref. [81]. The results we obtain indicate that, even though small, current bounds on neutrino magnetic moments and solar magnetic fields still leave room for slight modifications in the determinations of solar neutrino oscillation parameters, in the presence of non-zero magnetic moments ⁴.

Turning to the general Majorana case, where theory may give rise to higher moments, there is a characteristic feature of the spin-flavor precession which will lead to more stringent constraints, and hence increase the robustness of the oscillation parameter determination. The argument is based on the presence of anti-neutrinos in the solar flux [76, 77, 78]. Recently the KamLAND collaboration [82] has reported a result which greatly improves the bound on an anti-neutrino component in the solar flux from 0.1% of the solar boron-8 flux to

⁴ Note that our analysis of solar neutrino data applies also to the special case of Dirac neutrinos.

$2.8 \cdot 10^2 \%$ at the 90% C.L., about 30 times better than the recent Super-K limit [83]. This implies that, in practical terms, extremely good stability of the solar neutrino oscillation parameters against the possible existence of sub-leading SFP conversions is obtained. As a result, we conclude that solar neutrinos oscillation parameters can be inferred without any reference to neutrino magnetic properties nor solar magnetic fields. We refer the reader to Ref. [79] for quantitative details.

All in all, we note that our analysis of solar neutrino data implies that in practice we have a pretty good stability of the oscillation parameter determination for the case of Majorana neutrinos, due to the solar anti-neutrino limit from KamLAND. In contrast for the special case of Dirac neutrinos this limit does not apply and the determination of oscillation parameters is potentially more fragile. However, we note that the gauge theoretic expectations for Dirac magnetic moments are lower than those for Majorana neutrino transition moments.

3. Beyond SM neutrino cross sections: Constraining neutrino magnetic moments

Neutrino transition magnetic moments are basic properties of neutrinos [76]. Although they do not substantially affect neutrino propagation, even in the presence of solar magnetic fields, non-trivial electromagnetic neutrino properties could still show up in the detection process and to this extent affect the determination of oscillation parameters. Experiments based on the neutrino detection via neutrino-electron elastic scattering are a sensitive probe of the electromagnetic properties. In Ref. [84] it was shown that current data from solar neutrinos (in particular from Super-K) in combination with reactor neutrino-electron scattering data provides strong bounds on all the elements of the TM matrix (for similar analyses see Ref. [85, 86, 87, 88]).

In several experiments such as Super-K, Borexino and some reactor experiments [89, 90, 91], neutrinos are detected via the elastic neutrino-electron scattering, whose electromagnetic cross section is [92, 93]

$$\frac{d\sigma_{em}}{dT} = \frac{2}{m_e^2} \frac{1}{T} \frac{1}{E} \frac{2}{e}; \quad (11)$$

where e is an effective MM [94], T denotes the kinetic energy of the recoil electron and E is the incoming neutrino energy. The electromagnetic cross section adds to the weak cross section and allows to extract information on the TM matrix, which we denote by σ in the following. Taking into account the antisymmetry of σ for Majorana neutrinos, it is useful to define vectors $\sigma_{jk} = \sigma_{jk1}$, where σ_{jk} are the elements of the TM matrix in the mass basis. The effective MM square σ_e^2 takes on different forms in the cases of solar and reactor neutrino experiments. The detailed derivation of the following expressions can be found in

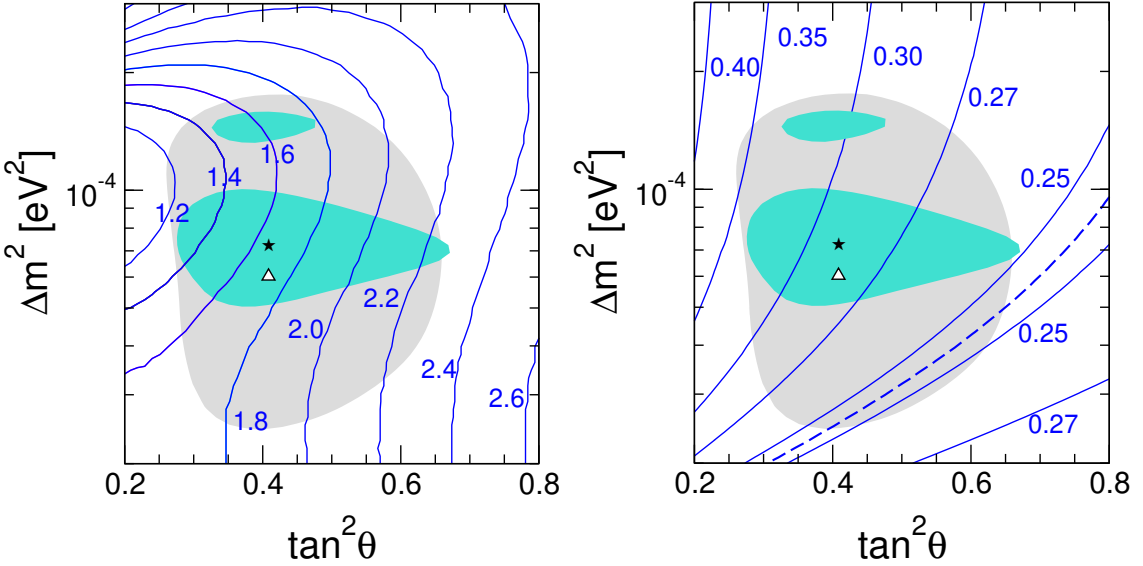


Figure 11: Contours of the 90% C.L. bound on $j \bar{j}$ in units of $10^{-10} B$ from combined solar and reactor data (left panel) and after 3 years of Borexino data-taking (right panel). The gray (light) shaded region is the 3-LMA region obtained in the global analysis of solar neutrino data (best fit point marked with a triangle), whereas the green (dark) one corresponds to the 3-LMA region obtained after including the KamLAND results (best fit point marked with a star). The dashed line in the right panel corresponds to $P_{e1} = 0.5$ for ${}^7\text{Be}$ neutrinos, and shows the strongest attainable limit.

Ref. [84]. For the case of solar neutrino experiments one obtains the effective MM square

$${}_{\text{LMA}}^2 = j_1^2 + j_2^2 + P_{e1}^2 j_2^2 - j_1^2 ; \quad (12)$$

where P_{e1}^2 corresponds to the probability that an electron neutrino produced in the core of the sun arrives at the detector as the mass eigenstate ${}_1$ in a two-neutrino scheme. The ${}_{\text{e}}^2$ relevant in reactor experiments is given as

$${}_{\text{R}}^2 = j_1^2 \cos^2 {}_{\text{sol}} j_1^2 + \sin^2 {}_{\text{sol}} j_2^2 - \sin 2 {}_{\text{sol}} j_1 j_2 \cos ; \quad (13)$$

where $\phi = \arg(j_1 j_2)$ is the relative phase between j_1 and j_2 .

In the following we discuss the constraints on neutrino TMs from solar and reactor neutrino experiments [84]. The 2 obtained from the data is minimized with respect to all TM parameters except the modulus $j \bar{j}$. To take into account the physical boundary $j \bar{j} = 0$ we use Bayesian methods to calculate an upper bound on $j \bar{j}$. Let us stress that these bounds apply to all elements of the TM matrix, including MMs and electric dipole moments of all neutrino flavours, since $j \bar{j}^2 = j_1^2 + j_2^2 + j_3^2$. Furthermore, since $j \bar{j}$ is independent of the basis these bounds apply also for the TMs in the flavour basis.

In the left panel of Fig. 11 we show contours of the 90% C.L. bound on $j \bar{j}$ in the $(\tan^2 {}_{\text{sol}}; m_{\text{sol}}^2)$ plane for the combination of solar and reactor data. We note that in the

upper parts of the LM A region, the solar data alone give already a strong bound on j , see Ref. [84] for details. In contrast, for low m_{sol}^2 values the inclusion of reactor data plays an important role in improving the bound. From our analysis we find at 90% C.L.:

$$\begin{aligned} j < 4.0 \cdot 10^{10} & \text{ B (solar + KamLAND data)} \\ 1.8 \cdot 10^{10} & \text{ B (solar + KamLAND + reactor data),} \end{aligned} \quad (14)$$

where for each value of j we have minimized the χ^2 with respect to \tan^2_{sol} and m_{sol}^2 .

Finally we note that the Borexino experiment [95] will improve these bounds roughly by one order of magnitude. This experiment is mainly sensitive to the solar ${}^7\text{Be}$ neutrino flux, which will be measured by elastic neutrino-electron scattering. Therefore, Borexino is similar to Super-K, the main difference is the mono-energetic line of the ${}^7\text{Be}$ neutrinos, with an energy of 0.862 MeV, which is roughly one order of magnitude smaller than the energies of the ${}^8\text{B}$ neutrino flux relevant in Super-K. Thanks to the lower neutrino energy the sensitivity to electromagnetic properties is increased, as can be seen from Eq. (11). Details about our Borexino simulation can be found in Ref. [84]. At the best t point one finds the sensitivity

$$j < 0.28 \cdot 10^{10} \text{ B at 90% C.L.} \quad (15)$$

after three years of Borexino data taking. In the right panel of Fig. 11 we show contours of the 90% C.L. bound in the $(\tan^2_{sol}; m_{sol}^2)$ plane.

IV. THREE-FLAVOUR NEUTRINO OSCILLATIONS

A. Global three-neutrino analysis

In this section the three-neutrino oscillation parameters are determined from a global analysis of the most recent neutrino oscillation data. For earlier three-neutrino analyses see Refs. [33, 96, 97]. To fix the notation, we define the neutrino mass-squared differences $m_{sol}^2 - m_{21}^2 - m_2^2 - m_1^2$ and $m_{atm}^2 - m_{31}^2 - m_3^2 - m_1^2$, and use the convenient form of the parameterization for the leptonic mixing matrix given in Ref. [18] and now adopted as standard by the PDG [98]:

$$U = \begin{pmatrix} 0 & & & & & 1 \\ & c_{13}c_{12} & & s_{12}c_{13} & & s_{13} \\ & s_2c_{23} & s_3s_{13}c_{12} & c_{23}c_{12} & s_3s_{13}s_{12} & s_{23}c_{13} \\ \hline B & & & & & A \\ s_2c_{23} & s_3s_{13}c_{12} & c_{23}c_{12} & s_3c_{12} & s_3s_{12}c_{23} & c_{23}c_{13} \end{pmatrix}; \quad (16)$$

where $c_{ij} = \cos \theta_{ij}$ and $s_{ij} = \sin \theta_{ij}$. Furthermore, we use the notations $\theta_{12} = \theta_{sol}$ and $\theta_{23} = \theta_{atm}$. Because of the hierarchy $m_{sol}^2 \ll m_{atm}^2$ it is a good approximation to set $m_{sol}^2 = 0$ in the analysis of atmospheric and K2K data⁵, and to set m_{atm}^2 to infinity for the analysis

⁵ See Ref. [99] for a two-mass scale analysis of atmospheric data.

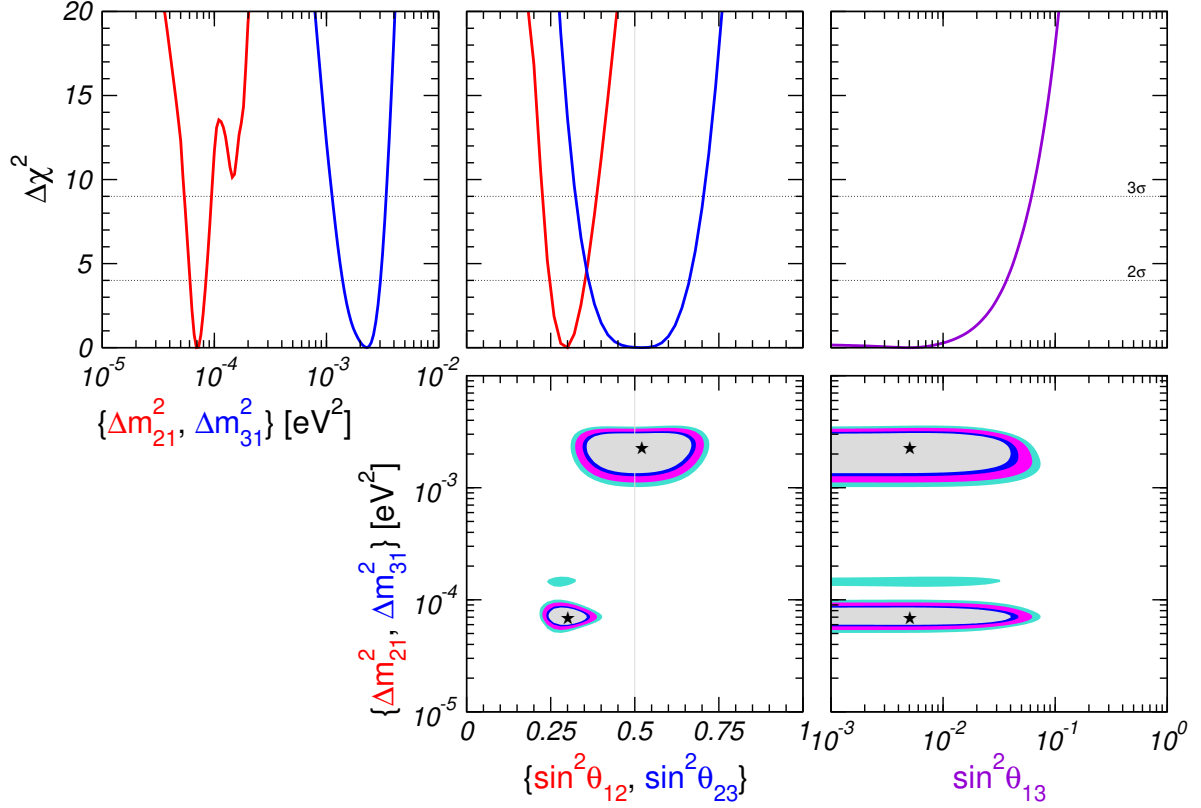


Figure 12: Projections of the allowed regions from the global oscillation data at 90%, 95%, 99%, and 3 C.L. for 2 d.o.f. for various parameter combinations. Also shown is $\Delta\chi^2$ as a function of the oscillation parameters $\sin^2 \theta_{12}$; $\sin^2 \theta_{23}$; $\sin^2 \theta_{13}$; Δm^2_{21} ; Δm^2_{31} , minimized with respect to all undisplayed parameters.

of solar and KamLAND data. This implies furthermore that the effect of a possible Dirac CP-violating phase [18] in the lepton mixing matrix can be neglected⁶. We perform a general fit to the global data in the five-dimensional parameter space $\sin^2 \theta_{12}; \sin^2 \theta_{23}; \sin^2 \theta_{13}; \Delta m^2_{21}; \Delta m^2_{31}$, and show projections onto various one- or two-dimensional sub-spaces.

We include in our analysis the global solar neutrino oscillation data from all solar neutrino experiments and the KamLAND reactor experiment as described in Sec. III, the atmospheric neutrino data from Super-K, as well as the first spectral data from the K2K long-baseline experiment (see Sec. II). In addition we take into account in our fit the constraints from the CHOOZ reactor experiment [101].

The results of the global three-neutrino analysis are summarized in Fig. 12 and in Tab. I. In the upper panels of the figure the $\Delta\chi^2$ is shown as a function of the parameters

⁶ The two Majorana phases [18] do not show up in oscillations but do appear in lepton number violating processes [100].

parameter	best t	2	3	5
$m_{21}^2 [10^{-5} \text{ eV}^2]$	6.9	6.1{8.4}	5.4{9.4}	2.1{29}
$m_{31}^2 [10^{-3} \text{ eV}^2]$	2.3	1.4{3.0}	1.1{3.4}	0.68{4.4}
$\sin^2 \theta_{12}$	0.30	0.25{0.35}	0.23{0.39}	0.16{0.47}
$\sin^2 \theta_{23}$	0.52	0.36{0.66}	0.32{0.70}	0.26{0.78}
$\sin^2 \theta_{13}$	0.005	0.037	0.061	0.13

Table I: Best- t values, 2, 3, and 5 intervals (1 d.o.f.) for the three-flavour neutrino oscillation parameters from global data including solar, atmospheric, reactor (KamLAND and CHOOZ) and accelerator (K2K) experiments.

eters $\sin^2 \theta_{12}$; $\sin^2 \theta_{23}$; $\sin^2 \theta_{13}$; m_{21}^2 ; m_{31}^2 , minimized with respect to the undisplayed parameters. The lower panels show two-dimensional projections of the allowed regions in the three-dimensional parameter space. The best- t values and the allowed ranges of the oscillation parameters from the global data are given in Tab. I. This table summarizes the current status of the three-flavour neutrino oscillation parameters.

B. The small parameters $m_{\text{sol}}^2 = m_{\text{atm}}^2$ and θ_{13}

Genuine three-flavour effects are associated to the mass hierarchy parameter $m_{\text{sol}}^2 = m_{\text{atm}}^2$ and the mixing angle θ_{13} . In particular, in a three-neutrino scheme CP violation disappears in the limit where two neutrinos become degenerate [18, 102] and in the limit where $\theta_{13} \rightarrow 0$. We discuss in this subsection the present status of these small parameters.

In Fig. 13 the χ^2 from the global data is shown as a function of the mass hierarchy parameter. Also shown in this figure is the χ^2 as a function of the parameter combination $\sin^2 \theta_{12}$, since to leading order in the long baseline $\theta_{13} \rightarrow 0$. The oscillation probability solar parameters appear in this particular combination [103, 104]. We obtain the following best- t values and 3 intervals:

$$\begin{aligned} \theta_{13} &= 0.030; & 0.019 & & 0.066; \\ \sin^2 \theta_{12} &= 0.028; & 0.018 & & 0.060; \end{aligned} \quad (17)$$

Let us now discuss the status of the mixing angle θ_{13} , which at the moment is the last unknown angle in the three-neutrino leptonic mixing matrix. Only an upper bound exists, which used to be dominated by the CHOOZ [101] and Palo Verde [105] reactor experiments. Currently a large effort is put to determine this angle in future experiments (see, e.g., Refs. [24, 25, 106]).

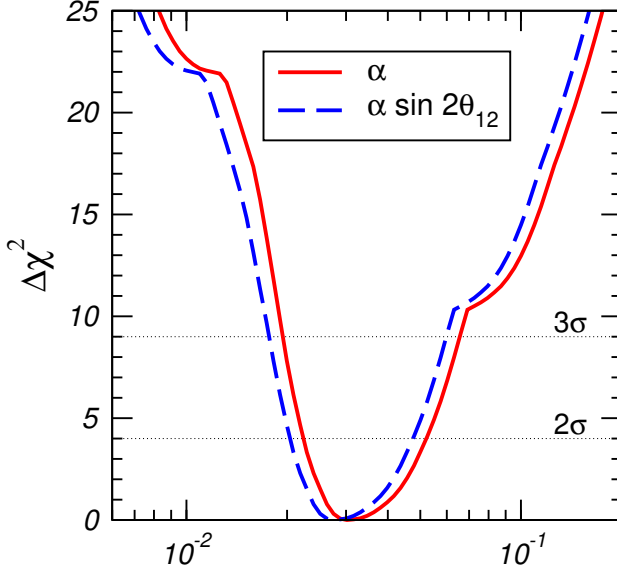


Figure 13: $\Delta\chi^2$ from global oscillation data as a function of $m_{\text{sol}}^2 = m_{\text{atm}}^2$ and $\sin 2\theta_{12}$.

In Fig. 14 we show the $\Delta\chi^2$ as a function of $\sin^2 \theta_{13}$ for different data sample choices. From this figure we find the following bounds at 90% C.L. (3 σ) for 1 d.o.f.:

$$\begin{aligned}
 \sin^2 \theta_{13} &\gtrsim 0.068 \text{ (0.12) } & (\text{solar+ KamLAND}) \\
 \sin^2 \theta_{13} &\gtrsim 0.031 \text{ (0.081) } & (\text{CHOOZ+ atm ospheric}) \\
 \sin^2 \theta_{13} &\gtrsim 0.029 \text{ (0.061) } & (\text{global data})
 \end{aligned} \tag{18}$$

One observes that the bound on $\sin^2 \theta_{13}$ from global data is dominated by the CHOOZ reactor experiment, together with the determination of m_{31}^2 from atmospheric data. However, it was noted in Ref. [28] that current solar data start to contribute significantly to the constraint on $\sin^2 \theta_{13}$. In particular, the relatively lower values of m_{atm}^2 implied by the use of the new three-dimensional atmospheric fluxes [30] lead to a loosening of the CHOOZ bound on $\sin^2 \theta_{13}$, since this bound deteriorates quickly when m_{atm}^2 decreases (see Fig. 15). This explains the slightly weaker bound from CHOOZ and atmospheric data in Eq. (18) compared to the 90% C.L. bound $\sin^2 \theta_{13} = 0.028$ obtained in Ref. [28], where slightly higher m_{atm}^2 values were found due to the use of the one-dimensional Bartol atmospheric neutrino fluxes.

Such loosening in sensitivity for low m_{atm}^2 is prevented to some extent by solar neutrino data. In Fig. 15 we show the upper bound on $\sin^2 \theta_{13}$ as a function of m_{atm}^2 from CHOOZ data alone compared to the bound from an analysis including solar and reactor neutrino data (CHOOZ and KamLAND). One finds that, although for larger m_{atm}^2 values the bound on $\sin^2 \theta_{13}$ is dominated by the CHOOZ data, for $m_{\text{atm}}^2 < 2 \times 10^3 \text{ eV}^2$ the solar+ KamLAND data start being important. We note that also the bound from solar data is rather stable

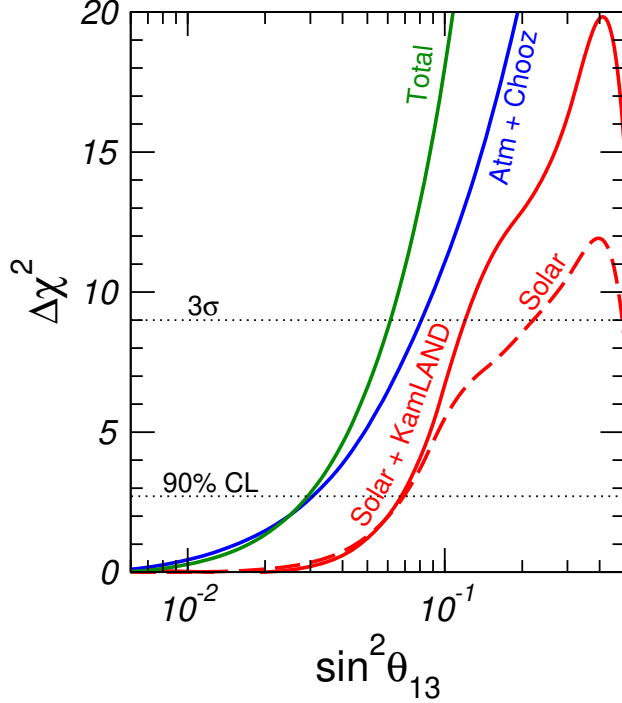


Figure 14: $\Delta\chi^2$ profiles projected onto the $\sin^2 \theta_{13}$ axis, for solar, solar+KamLAND, atmospheric+CHOOZ, and for the global data.

under the recent SSM update. The BP04 bound given in Eq. (18) has to be compared to the previous 90% C.L. bound $\sin^2 \theta_{13} = 0.070$ [28] implied by the BP00 SSM.

Let us discuss in some more detail the constraint on $\sin^2 \theta_{13}$ from solar data, which emerges from a subtle interplay of various solar neutrino observables. In Fig. 16 we show the results of a three parameter fit ($\sin^2 \theta_{\text{sol}}; m_{\text{sol}}^2, \sin^2 \theta_{13}$) to solar and KamLAND data. Allowed regions are shown for various values of $\sin^2 \theta_{13}$ in the $(\sin^2 \theta_{\text{sol}}; m_{\text{sol}}^2)$ plane with respect to the global minimum, which occurs for $\sin^2 \theta_{13} = 0.01$. Note that here we calculate the allowed regions at a given confidence level for 3 d.o.f. The shape of $\Delta\chi^2$ from solar data shown in Fig. 14 can be understood from Fig. 16. Indeed one observes that for solar data increasing θ_{13} can be compensated to some extent by increasing m_{sol}^2 . Since solar data disfavours large values of m_{sol}^2 the bound improves. Also KamLAND data acts in a similar way. Since the minimum around $m_{\text{sol}}^2 = 7 \times 10^5 \text{ eV}^2$ is preferred the continuous rise of m_{sol}^2 is prevented to some extent, and the "jump" of the local minimum into the high-LMA region occurs at larger values of $\sin^2 \theta_{13}$.

The difference in the day/night solar neutrino fluxes due to the regeneration effect in the earth in the three-flavour framework has been considered recently in Refs. [107, 108]. This observable may provide valuable information on θ_{13} in the context of future solar neutrino experiments like UNO or Hyper-K [109].

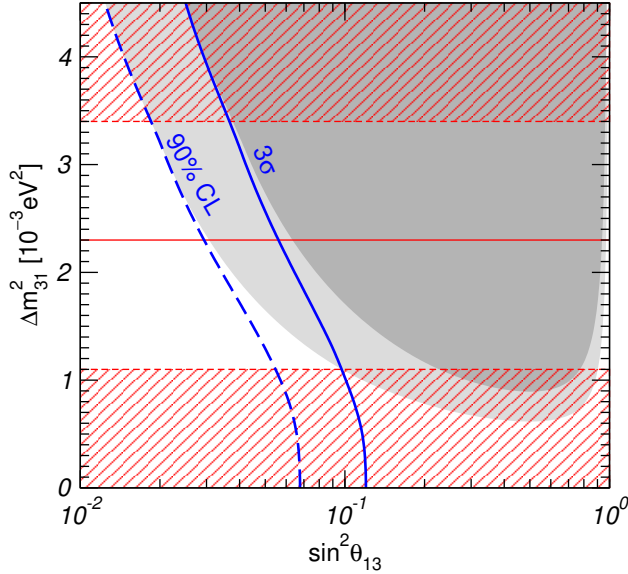


Figure 15: Upper bound on $\sin^2 \theta_{13}$ (1 d.o.f.) from solar+KamLAND+CHOOZ data as a function of m_{atm}^2 . The dashed (solid) curve corresponds to the 90% (3%) C.L. bound, the light (dark) shaded region is excluded by CHOOZ data alone at 90% (3%) C.L.. The horizontal line corresponds to the best t value of m_{atm}^2 within the 3-dimensional atmospheric model of Ref. [30] given in Eq. (2), and the hatched regions are excluded by atm ospheric + K2K data at 3 according to Eq. (3).

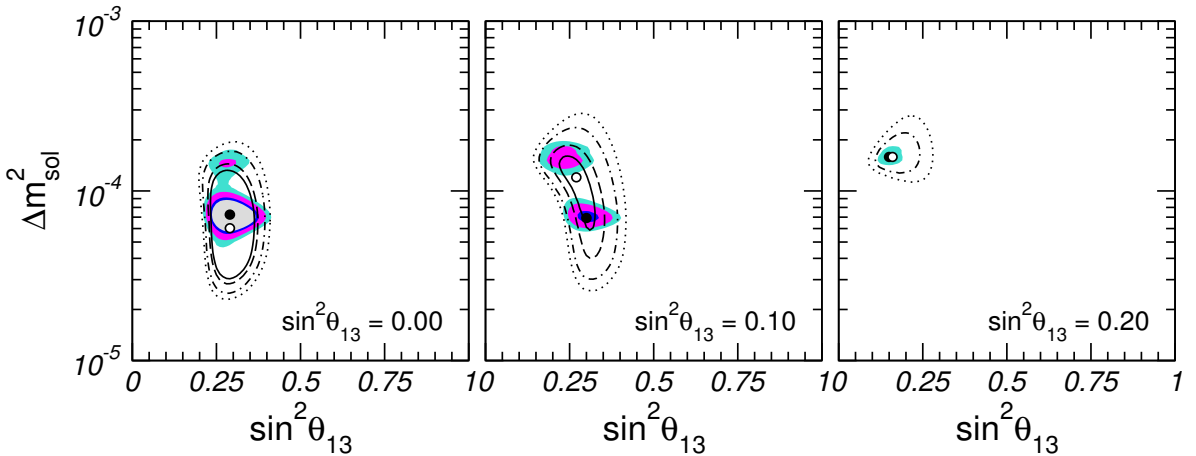


Figure 16: Sections of the three-dimensional allowed regions in the $(\sin^2 \theta_{13}; m_{\text{sol}}^2)$ plane at 90%, 95%, 99% and 3 C.L. for 3 d.o.f. for various $\sin^2 \theta_{13}$ values from solar data (lines) and solar+KamLAND data (colored regions). The local minima in each plane from solar+KamLAND (solar only) data are marked by filled (open) dots.

V. FOUR-NEUTRINO OSCILLATIONS AND LSND

In addition to the strong evidence for oscillations due to the mass-squared differences m_{sol}^2 and m_{atm}^2 there comes also a hint for oscillations with a much larger mass-squared difference from the LSND experiment [110]. This accelerator experiment performed at Los Alamos observed 87.9 \pm 22.4 \pm 6.0 excess events in the $\bar{\nu}_e \rightarrow \nu_e$ appearance channel, corresponding to a transition probability of $P = (0.264 \pm 0.067 \pm 0.045)\%$, which is 3.3 away from zero. To explain this signal with neutrino oscillations requires a mass-squared difference $m_{lsnd}^2 \approx 1 \text{ eV}^2$. Such a value is inconsistent with the mass-squared differences required by solar/KamLAND and atmospheric/K2K experiments within the standard three-flavour framework. In this section we consider four-neutrino schemes, where a sterile neutrino [111, 112, 113] is added to the three active ones to provide the additional mass scale needed to reconcile the LSND evidence. We include in our analysis all the data from solar, atmospheric and KamLAND neutrino experiments, the LSND experiment, as well as data from short-baseline (SBL) accelerator [114, 115] and reactor [101, 105, 116] experiments reporting no evidence for oscillations.

A. A comparison parametrization for four-neutrino schemes

Four-neutrino mass schemes are usually divided into the two classes (3+1) and (2+2), as illustrated in Fig. 17. We note that (3+1) mass spectra include the three-active neutrino scenario as limiting case. In this case solar and atmospheric neutrino oscillations are explained by active neutrino oscillations, with mass-squared differences m_{sol}^2 and m_{atm}^2 , and the fourth neutrino state gets completely decoupled. We will refer to such limiting scenario as (3+0). In contrast, the (2+2) spectrum is intrinsically different, as the sterile neutrino must take part in either solar or in atmospheric neutrino oscillations, or in both.

Neglecting CP violation, neutrino oscillations in four-neutrino schemes are generally described by 9 parameters: 3 mass-squared differences and 6 mixing angles in the lepton mixing matrix [18]. We use the parametrization introduced in Ref. [117], in terms of m_{sol}^2 , θ_{sol} , m_{atm}^2 , θ_{atm} , m_{lsnd}^2 , θ_{lsnd} . These 6 parameters are similar to the two-neutrino mass-squared differences and mixing angles and are directly related to the oscillations in solar, atmospheric and the LSND experiments. For the remaining 3 parameters we use s_{θ_e} and d . These quantities are defined by

$$x = \sum_i \sin^2 \theta_i \quad \text{with } i \text{ solar mass states,} \quad (19)$$

$$d = 1 - \sum_i \sin^2 \theta_i \quad \text{with } i \text{ atmospheric mass states,} \quad (20)$$

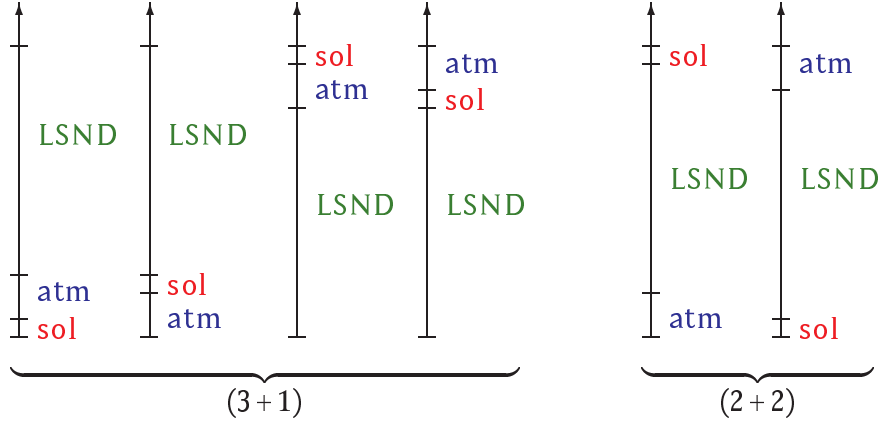


Figure 17: The two classes of six four-neutrino mass spectra, (3+1) and (2+2).

where $e = e; \nu_s; \nu_{atm}; \nu_{LSND}$. Note that in (2+2) scheme the relation $\nu_s = d$ holds, whereas in (3+1) and d are independent. The physical meaning of these parameters is the following: ν_s is the fraction of ν_e participating in solar oscillations, and $(1 - d)$ is the fraction of ν_{atm} participating in oscillations with m_{atm}^2 (for further discussions see Ref. [117]). For the analysis we adopt the following approximations:

1. We make use of the hierarchy $m_{sol}^2 \ll m_{atm}^2 \ll m_{LSND}^2$. This means that for each data set we consider only one mass-squared difference, the other two are set either to zero or to infinity.
2. In the analyses of solar and atm oscillations (but not for SBL data) we set $\nu_e = 1$, which is justified because of strong constraints from reactor experiments [101, 105, 116].

Within this approximation the parameter structure of the four-neutrino analysis gets rather simple. The parameter dependence of the four data sets solar, atm oscillations, LSND and NEV is illustrated in Fig. 18. The NEV data set contains the experiments KARMEN [114], CDS [115], Bugey [116], CHOOZ [101], and Palo Verde [105], reporting no evidence for oscillations. We see that only ν_s links solar and atm oscillations data and d links atm oscillations and NEV data, while LSND and NEV data are coupled by m_{LSND}^2 and m_{NEV}^2 . With the definitions (19) and (20) and in our approximation the parameter structure shown in Fig. 18 holds for both types of mass spectra, (3+1) as well as (2+2) [117].

B. (2+2): ruled out by solar and atm oscillations data

The strong preference for oscillations into active neutrinos in solar and atm oscillations [34] leads to a direct constraint in (2+2) oscillation schemes. We will now show that

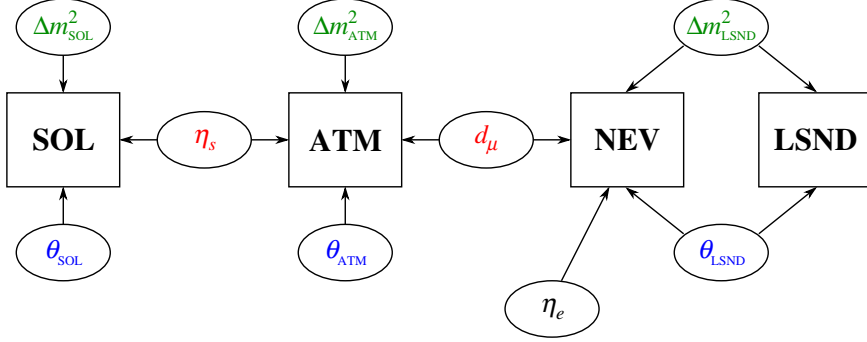


Figure 18: Parameter dependence of the different data sets in our parametrization.

thanks to recent solar neutrino data (in particular from the SNO-salt phase [10]) in combination with the KamLAND experiment [14], and the latest Super-K data on atmospheric neutrinos [11] the tension in the data has become so strong that (2+2) oscillation schemes are essentially ruled out⁷.

In the left panel of Fig. 19 we show the χ^2 from solar neutrino data as a function of η_s , the parameter describing the fraction of the sterile neutrino participating in solar neutrino oscillations. It is clear from the figure that the improved determination of the neutral current event rate from the solar ${}^8\text{B}$ flux implied by the salt enhanced measurement in SNO [10] substantially tightened the constraint on a sterile contribution: The 99% C.L. bound improves from $\eta_s = 0.44$ for pre-SNO-salt to $\eta_s = 0.31$ (BP00). The boron flux predicted in the current BP04 SSM is slightly larger than the NC flux measured in SNO, which leaves more room for a sterile component in the solar neutrino flux. Indeed, using the BP04 SSM the bound deteriorates slightly to $\eta_s = 0.36$ at the 99% C.L.. This effect illustrates that in schemes beyond minimal three-flavour oscillations the data still shows some sensitivity to the theoretical SSM input. Although KamLAND on its own is insensitive to a sterile neutrino contamination, it contributes indirectly to the bound because of the better determination of m_{sol}^2 and θ_{sol} [34]. The combined analysis leads to the 99% C.L. bound

$$\eta_s = 0.29 \quad (\text{solar + KamLAND, BP04}). \quad (21)$$

In contrast, in (2+2) schemes atmospheric data prefer values of η_s close to 1. From the combined analysis of SuperK and MACRO atmospheric data, and SBL neutrino data we obtain the bound $\eta_s = 0.70$ at 99% C.L., in clear disagreement with the bound from solar data. In the right panel of Fig. 19 we show the χ^2 for solar data and for atmospheric combined with SBL data as a function of η_s . Furthermore, we show the χ^2 of the global

⁷ For an earlier four-neutrino analysis of solar and atmospheric data see Ref. [118].

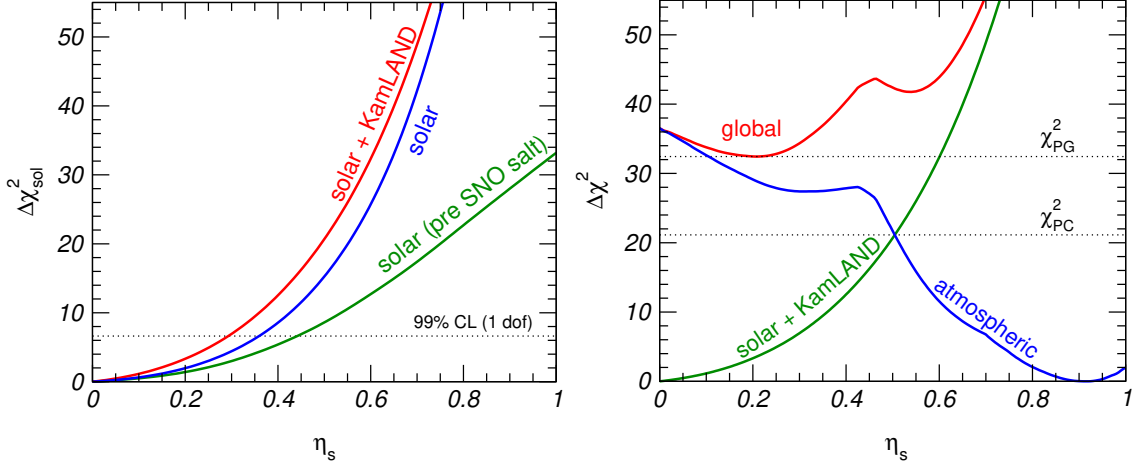


Figure 19: Left: $\Delta\chi^2$ as a function of η_s from solar data before the SNO salt-phase results, from current solar data, and from solar+KamLAND data. Right: $\Delta\chi^2_{\text{sol}}$, $\Delta\chi^2_{\text{atm+sb1}}$ and $\Delta\chi^2_{\text{global}}$ as a function of η_s in (2+2) oscillation schemes.

data defined by

$$\chi^2(\eta_s) = \chi^2_{\text{sol}}(\eta_s) + \chi^2_{\text{atm+sb1}}(\eta_s); \quad (22)$$

From the figure we find that only at the 4.6 level a value of η_s exists, which is contained in the allowed regions of both data sets. This follows from the χ^2 -value $\chi^2_{\text{PC}} = 21.1$ shown in the figure. In Refs. [119, 120] we have proposed a statistical method to evaluate the disagreement of different data sets in global analyses. The parameter goodness of fit (PG) makes use of the χ^2 defined in Eq. (22). This criterion evaluates the GOF of the combination of data sets, avoiding dilution by the large number of data points, as it happens for the usual GOF criterion (for details see Ref. [120]). We find $\chi^2_{\text{PG}} = \chi^2_{\text{min}} = 32.4$, which corresponds to 5.7. We conclude that (2+2) mass schemes are ruled out by the disagreement between the latest solar and atmospheric neutrino data. This is a very robust result, independent of whether LSND is confirmed or disproved⁸.

C. (3+1): strongly disfavoured by SBL data

It is known for a long time [124, 125, 126, 127, 128, 129, 130] that (3+1) mass schemes are disfavoured by the comparison of SBL disappearance data [115, 116] with the LSND

⁸ Sub-leading effects beyond the approximations adopted here should not affect this result significantly. Allowing for additional parameters to vary at the percent level might change the ratio of some observables [121], however, we expect that the absolute number of events relevant for the fit will not change substantially.

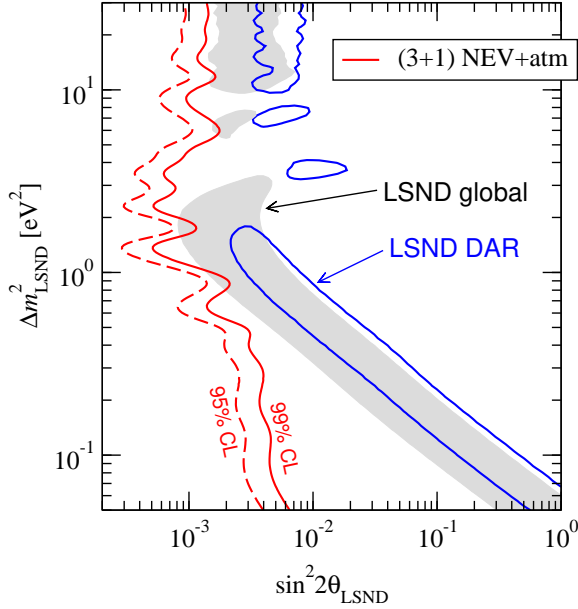


Figure 20: Upper bound on $\sin^2 2\theta_{\text{LSND}}$ from NEV and atmospheric neutrino data in (3+1) schemes [122] compared to the allowed region from global LSND data [110] and decay-at-rest (DAR) LSND data [123].

result. In Ref. [122] an upper bound on the LSND oscillation amplitude $\sin^2 2\theta_{\text{LSND}}$ was obtained from NEV and atmospheric neutrino data. From Fig. 20 we see that this bound is incompatible with the signal observed in LSND at the 95% CL. Only marginal overlap regions exist between the bound and global LSND data if both are taken at 99% CL. Using only the decay-at-rest LSND data sample [123] the disagreement is even more severe. An analysis in terms of the parameter goodness of fit [119] shows that for most values of Δm_{LSND}^2 NEV and atmospheric data are compatible with LSND only at more than 3%, unless $\Delta m_{\text{LSND}}^2 > 6 \text{ eV}^2$, where the PG reaches 1%. These results show that (3+1) schemes are strongly disfavoured by SBL disappearance data.

D. Comparing (3+1), (2+2) and (3+0) hypotheses

Using the methods developed in Ref. [117] we perform a global fit to the oscillation data in the four-neutrino framework. This approach allows to statistically compare the different hypotheses. Let us first evaluate the GOF of (3+1) and (2+2) spectra using the PG method described in Ref. [120]. We divide the global oscillation data into the four data sets SO L, ATM, LSND and NEV. Following Ref. [119] we consider

$$\chi^2 = \chi^2_{\text{sol}}(\text{sol}; \Delta m_{\text{sol}}^2; s) + \chi^2_{\text{atm}}(\text{atm}; \Delta m_{\text{atm}}^2; s; d) + \chi^2_{\text{nev}}(\text{lsnd}; \Delta m_{\text{lsnd}}^2; d; e) + \chi^2_{\text{lsnd}}(\text{lsnd}; \Delta m_{\text{lsnd}}^2); \quad (23)$$

	SOL	ATM	LSND	NEV	$\frac{2}{PG}$	PG	
(3+1)	0.0	0.4	7.2	7.0	14.6	5.6	10^{-3} (2.8)
(2+2)	3.5	29.0	1.2	9.7	43.4	8.5	10^{-9} (5.8)

Table II: Parameter GOF and the contributions of different data sets to $\frac{2}{PG}$ in (3+1) and (2+2) neutrino mass schemes.

where $\frac{2}{X} = \frac{2}{X} (\frac{2}{X})_{\text{min}}$ ($X = \text{SOL, ATM, NEV, LSND}$). In Tab. II we show the contributions of the 4 data sets to $\frac{2}{PG}$ $\frac{2}{\text{min}}$ for (3+1) and (2+2) oscillation schemes. As expected we observe that in (3+1) schemes the main contribution comes from SBL data due to the tension between LSND and NEV data in these schemes. For (2+2) oscillation schemes a large part of $\frac{2}{PG}$ comes from solar and atm ospheric data, with a significant contribution from SBL data. The latter comes mainly from the tension between LSND and KARMEN [123], which does not depend on the mass scheme.

The parameter goodness of t is now obtained by evaluating $\frac{2}{PG}$ for 4 d.o.f. [120]. This number of degrees of freedom corresponds to the 4 parameters $s; d; m_{\text{lsnd}}; m_{\text{lsnd}}$ describing the coupling of the different data sets (see Eq. (23) and Fig. 18). The best GOF is obtained in the (3+1) case. However, even in this best case the PG is only 0.56%. The PG of $8.5 \cdot 10^{-9}$ for (2+2) schemes shows that these mass schemes are essentially ruled out by the disagreement between the individual data sets.

Although we have seen that none of the four-neutrino mass schemes provides a good t to the global oscillation data including LSND, it is interesting to consider the relative status of the three hypotheses (3+1), (2+2) and the three-active neutrino scenario (3+0). This can be done by comparing the χ^2 values of the best t point (which occurs for the (3+1) scheme) with the one corresponding to (2+2) and (3+0). First we observe that (2+2) schemes are strongly disfavoured with respect to (3+1) with a $\chi^2 = 28.8$. For 4 d.o.f. this is equivalent to an exclusion at 4.5%. Furthermore, we find that (3+0) is disfavoured with a $\chi^2 = 20.0$ (99.95% C.L. for 4 d.o.f.) with respect to (3+1). This reflects the high statistical significance of the LSND result, since in a (3+0) no effect is predicted for LSND.

To summarize, we find that four-neutrino schemes do not provide a satisfactory t to the global data. The strong rejection of non-active oscillation in the solar+KamLAND and atm ospheric neutrino data rules out (2+2) schemes, irrespective of whether LSND is confirmed or not. Using an improved goodness of t method especially sensitive to the combination of data sets we find that (2+2) schemes are ruled out at the 5.8% level. On the other hand (3+1) spectra are disfavoured by the disagreement of LSND with short-baseline disappearance data, leading to a marginal GOF of $5.6 \cdot 10^{-3}$ (2.8%). Should LSND be confirmed it would be very desirable to have more data on ν_e and/or SBL disappearance

to decide about the status of (3+1) schemes. In that case a positive signal is predicted right at the sensitivity edge of existing experiments.

More drastic attempts to reconcile the LSND signal with the rest of neutrino oscillation data have been reviewed in Ref. [24]. For example, it has been shown in Ref. [131] that even the rather drastic assumption of CPT violation in a three-neutrino framework [132, 133] does not provide a satisfactory description of the global neutrino data set including LSND. Similarly, an interpretation of the LSND signal in terms of a non-standard muon decay is disfavoured by KARMEN [134].

We conclude that currently no convincing explanation for the LSND result exists, and it remains a puzzle how to reconcile this evidence with the rest of the global data. It is therefore very important to settle this issue experimentally. A confirmation of the LSND signal by the MiniBooNE experiment [135] would be very exciting and would require some novel physics ideas.

VI. SUMMARY AND CONCLUSIONS

We have given a brief review of the status of global analyses of neutrino oscillations, taking into account the latest neutrino data and state-of-the-art solar and atmospheric neutrino flux calculations. This included two-neutrino solar + KamLAND results, as well as two-neutrino atmospheric + K2K oscillation regions, and a discussion in each case of the robustness with which the oscillation hypothesis can be established, in view of possible modifications. These might come from the assumed theoretical fluxes, the non-validity of the Standard Model neutrino interaction cross sections or the existence of non-trivial neutrino propagation properties beyond oscillations. As case studies we have mentioned the robustness of the solar neutrino oscillation hypothesis vis-à-vis the possible existence of radiative-zone solar density fluctuations, nonzero convective-zone solar magnetic fields and neutrino transition magnetic moments. For the atmospheric + K2K analysis we have considered explicitly the robustness of the oscillation hypothesis against the possible existence of flavour or universality violating non-standard neutrino interactions.

Furthermore, we have performed a fit to the most recent world neutrino data sample in the three-flavour framework. The results of this global analysis are summarized in Fig. 12 and Tab. I, where we give the best-fit values and allowed ranges of the three-flavour oscillation parameters. In addition we discussed in detail the status of the small parameters

$m_{\text{sol}}^2 = m_{\text{atm}}^2$ and $\sin^2 \theta_{13}$, which characterize the strength of CP violating effects in neutrino oscillations. Finally, we gave a review over the current status of four-neutrino interpretations of the LSND anomaly, in view of the most recent experimental and theoretical advances.

All in all, we can say beyond reasonable doubt that neutrino masses, discovered through atmospheric neutrino oscillations, have now also been confirmed in the solar neutrino oscillation channel thanks to the important input of the KamLAND experiment. Theory-wise, while the SSM was necessary in order to establish the need for physics beyond the Standard Model, it has now been made irrelevant by the high precision of the experiments which currently dominate the determination of solar neutrino oscillation parameters. The next goal in the agenda is the determination of the small parameters $\sin^2 \theta_{13}$ and $m_{sol}^2 = m_{atm}^2$ that characterize the strength of CP violating effects in neutrino oscillations and the exploration of the Majorana nature of the neutrino which will be sensitive to the other leptonic CP phases.

Acknowledgments

This work was supported by Spanish grant BFM 2002-00345, by the European Commission RTN grant HPRN-CT-2000-00148 and the ESF Neutrino Astrophysics Network. M.M. is supported by the National Science Foundation grant PHY 0098527. T.S. has been supported by the \Sonderforschungsbereich 375 für Astro-Teilchenphysik der Deutschen Forschungsgemeinschaft". M.T. has been supported by FPU fellowship AP 2000-1953.

- [1] R. D avis, *Prog. Part. Nucl. Phys.* **32**, 13 (1994).
- [2] B. T. C leveland et al., *Astrophys. J.* **496**, 505 (1998).
- [3] SAGE Collaboration, J. N. Abdurashitov et al., *Phys. Rev. C* **60**, 055801 (1999), [[astro-ph/9907113](#)].
- [4] GNO Collaboration, C. M. Cattadori, *Nucl. Phys. Proc. Suppl.* **110**, 311 (2002).
- [5] GALLEX Collaboration, W. H ampe et al., *Phys. Lett. B* **447**, 127 (1999).
- [6] GNO Collaboration, M. A ltmann et al., *Phys. Lett. B* **490**, 16 (2000), [[hep-ex/0006034](#)].
- [7] Super-K amiookande Collaboration, S. Fukuda et al., *Phys. Lett. B* **539**, 179 (2002), [[hep-ex/0205075](#)].
- [8] SNO Collaboration, Q. R. A hm ad et al., *Phys. Rev. Lett.* **89**, 011301 (2002), [[nucl-ex/0204008](#)].
- [9] SNO Collaboration, Q. R. A hm ad et al., *Phys. Rev. Lett.* **89**, 011302 (2002), [[nucl-ex/0204009](#)].
- [10] SNO Collaboration, S. N. A hm ed et al., *Phys. Rev. Lett.*, 041801 (2003), [[nucl-ex/0309004](#)].
- [11] Super-K amiookande Collaboration, Y. Fukuda et al., *Phys. Rev. Lett.* **81**, 1562 (1998),

[hep-ex/9807003].

[12] MACRO Collaboration, A. Surdo, Nucl. Phys. Proc. Suppl. 110, 342 (2002).

[13] Soudan 2 Collaboration, M. Sanchez et al., Phys. Rev. D 68, 113004 (2003), [hep-ex/0307069].

[14] KamLAND Collaboration, K. Eguchi et al., Phys. Rev. Lett. 90, 021802 (2003), [hep-ex/0212021].

[15] K2K Collaboration, M. H. Ahn et al., Phys. Rev. Lett. 90, 041801 (2003), [hep-ex/0212007].

[16] M. Gell-Mann, P. Ramond and R. Slansky, (1979), Print-80-0576 (CERN).

[17] T. Yanagida, (KEK lectures, 1979), ed. Sawada and Sugamoto (KEK, 1979).

[18] J. Schechter and J.W. F. Valle, Phys. Rev. D 22, 2227 (1980).

[19] R.N. Mohapatra and G. Senjanovic, Phys. Rev. D 23, 165 (1981).

[20] For a short review see J.W. F. Valle, "Neutrino masses twenty-five years later," AIP Conf. Proc. 687 (2003) 16 [arXiv:hep-ph/0307192].

[21] See, for example, M. Goodman's Neutrino Oscillation Industry Web Page, <http://neutrinooscillation.org/>

[22] S.P. Mikheev and A.Y. Smirnov, Sov. J. Nucl. Phys. 42, 913 (1985).

[23] L.Wolfeinstein, Phys. Rev. D 17, 2369 (1978).

[24] S. Pakvasa and J.W. F. Valle, Proceedings of the Indian National Academy of Sciences, Part A : Vol. 70A, No. 1, p.189 – 222 (2004), Eds. D. Indumathi, M.V.N. M. Murthy and G. Rajasekaran [hep-ph/0301061]

[25] V. Barger, D. Marfatia and K. Whisnant, Int. J. Mod. Phys. E 12 (2003) 56

[26] M.C. Gonzalez-Garcia and Y. Nir, Rev. Mod. Phys. 75 (2003) 34

[27] G.L. Fogli et al., Proc. of International Workshop on Astroparticle and High Energy Physics, October 14 – 18, 2003, Valencia, Spain, published at JHEP, PRHEP-AHEP 2003/071, accessible from <http://ictpv.es/ahep/>.

[28] M. Maltoni, T. Schwetz, M.A. Tortola and J.W. F. Valle, Phys. Rev. D 68, 113010 (2003), [hep-ph/0309130].

[29] J. N. Bahcall and M. H. Pinsonneault, Phys. Rev. Lett. 93, 121301 (2004), [astro-ph/0402114].

[30] M. Honda, T. Kajita, K. Kasahara and S. Morikawa, astro-ph/0404457.

[31] Super-Kamiokande Collaboration, Y. Ashie, hep-ex/0404034.

[32] Y. Hayato, <http://eps2003.physik.rwth-aachen.de>.

[33] M. Gonzalez-Garcia, M. Maltoni, C. Pena-Garay and J.W. F. Valle, Phys. Rev. D 63, 033005 (2001), [hep-ph/0009350].

[34] M. Maltoni, T. Schwetz, M.A. Tortola and J.W. F. Valle, Phys. Rev. D 67, 013011 (2003), [hep-ph/0207227 v3 KamLAND -updated version].

[35] J. Kamada, PhD Thesis, University of Tokyo, 2002, available from the Web-page <http://www-sk.icrr.u-tokyo.ac.jp/doc/sk/pub/>.

[36] G. L. Fogli, E. Lisi, A. Marrone and D. Montanino, Phys. Rev. D 67, 093006 (2003), [hep-ph/0303064].

[37] G. Barr, T. K. Gaisser and T. Stanev, Phys. Rev. D 39, 3532 (1989).

[38] J. Schechter and J. W. F. Valle, Phys. Rev. D 25, 774 (1982). J. W. F. Valle, Phys. Lett. B 131, 87 (1983). G. B. Gelmini and J. W. F. Valle, Phys. Lett. B 142, 181 (1984). M. C. Gonzalez-Garcia and J. W. F. Valle, Phys. Lett. B 216, 360 (1989).

[39] S. Pakvasa and K. Tennakone, Phys. Rev. Lett. 28, 1415 (1972).

[40] A. Zee, Phys. Lett. B 93, 389 (1980).

[41] K. S. Babu, Phys. Lett. B 203, 132 (1988).

[42] R. N. Mohapatra and J. W. F. Valle, Phys. Rev. D 34, 1642 (1986).

[43] L. J. Hall, V. A. Kostelecky and S. Raby, Nucl. Phys. B 267, 415 (1986).

[44] J. Bernabeu et al., Phys. Lett. B 187, 303 (1987).

[45] G. C. Branco, M. N. Rebelo and J. W. F. Valle, Phys. Lett. B 225, 385 (1989).

[46] N. Rius and J. W. F. Valle, Phys. Lett. B 246, 249 (1990).

[47] N. Fornengo et al., Phys. Rev. D 65, 013010 (2002), [hep-ph/0108043].

[48] J. W. F. Valle, Prog. Part. Nucl. Phys. 26, 91 (1991).

[49] M. Hirsch and J. W. F. Valle, hep-ph/0405015.

[50] M. C. Gonzalez-Garcia and M. Maltoni, hep-ph/0404085.

[51] H. Nunokawa, Y. Z. Qian, A. Rossi and J. W. F. Valle, Phys. Rev. D 54, 4356 (1996), [hep-ph/9605301].

[52] G. L. Fogli, E. Lisi, A. Marrone and D. Montanino, Phys. Rev. D 66, 013009 (2002), [hep-ph/0202269].

[53] D. Grasso, H. Nunokawa and J. W. F. Valle, Phys. Rev. Lett. 81, 2412 (1998), [astro-ph/9803002].

[54] A. McDonald, this volume.

[55] J. N. Bahcall and C. Pena-Garay, hep-ph/0404061.

[56] E. Bellotti and V. Gavrin, <http://moda.phys.washington.edu/>.

[57] SAGE Collaboration, J. N. Abdurashitov et al., J. Exp. Theor. Phys. 95, 181 (2002), [astro-ph/0204245].

[58] G. L. Fogli, E. Lisi, A. Marrone, D. Montanino and A. Palazzo, Phys. Rev. D 66, 053010 (2002), [hep-ph/0206162].

[59] A. B. Balantekin and H. Yuksel, Phys. Rev. D 68, 113002 (2003), [hep-ph/0309079].

[60] J. N. Bahcall, M. H. Pinsonneault and S. Basu, Astrophys. J. 555, 990 (2001),

[astro-ph/0010346].

- [61] P. Chankowski, A. Ioannissian, S. Pokorski and J. W. F. Valle, Phys. Rev. Lett. 86, 3488 (2001), [hep-ph/0011150].
- [62] G. Fiorentini, T. Lassner, M. Lissia, B. Ricci and S. Schonert, Phys. Lett. B 558, 15 (2003), [hep-ph/0301042].
- [63] H. Nunokawa, W. J. C. Teves and R. Zukanovich Funchal, JHEP 11, 020 (2003), [hep-ph/0308175].
- [64] T. Schwetz, Phys. Lett. B 577, 120 (2003), [hep-ph/0308003].
- [65] M. Maltoni, T. Schwetz and J. W. F. Valle, Phys. Rev. D 67, 093003 (2003), [hep-ph/0212129].
- [66] SuperKamiokande Collaboration, M. B. Smy et al., Phys. Rev. D 69, 011104 (2004), [hep-ex/0309011].
- [67] A. B. Balantekin, J. M. Fetter and F. N. Loret, Phys. Rev. D 54, 3941 (1996), [astro-ph/9604061].
- [68] H. Nunokawa, A. Rossi, V. B. Semikoz and J. W. F. Valle, Nucl. Phys. B 472, 495 (1996), [hep-ph/9602307].
- [69] P. Bamert, C. P. Burgess and D. M. Chaud, Nucl. Phys. B 513, 319 (1998), [hep-ph/9707542].
- [70] V. Castellani, S. Degl'Innocenti, W. A. Dziewolski, G. Fiorentini and B. Ricci, Nucl. Phys. Proc. Suppl. 70, 301 (1999), [astro-ph/9712174].
- [71] J. Christensen-Dalsgaard, Rev. Mod. Phys. 74, 1073 (2003), [astro-ph/0207403].
- [72] C. P. Burgess et al., Mon. Not. Roy. Astron. Soc. 348, 609 (2004), [astro-ph/0304462].
- [73] C. Burgess et al., Astrophys. J. 588, L65 (2003), [hep-ph/0209094].
- [74] C. P. Burgess et al., JCAP 0401, 007 (2004), [hep-ph/0310366].
- [75] K. Fujikawa and R. Shrock, Phys. Rev. Lett. 45, 963 (1980).
- [76] J. Schechter and J. W. F. Valle, Phys. Rev. D 24, 1883 (1981), Err. Phys. Rev. D 25, 283 (1982).
- [77] E. K. Akhmedov, Phys. Lett. B 213, 64 (1988).
- [78] C.-S. Lim and W. J. Marciano, Phys. Rev. D 37, 1368 (1988).
- [79] O. G. M iranda, T. I. Rashba, A. I. Rez and J. W. F. Valle, hep-ph/0311014.
- [80] V. A. Kutvitskii and L. S. Solov'ev, J. Exp. Theor. Phys. 78, 456 (1994).
- [81] O. G. M iranda et al., Nucl. Phys. B 595, 360 (2001), [hep-ph/0005259].
- [82] KamLAND Collaboration, K. Eguchi et al., Phys. Rev. Lett. 92, 071301 (2004), [hep-ex/0310047].
- [83] SuperKamiokande Collaboration, Y. Gando et al., Phys. Rev. Lett. 90, 171302 (2003), [hep-ex/0212067].

[84] W .G rimus et al., *Nucl. Phys. B* 648, 376 (2003), [[hep-ph/0208132](#)].

[85] J.F .Beacom and P .Vogel, *Phys. Rev. Lett.* 83, 5222 (1999), [[hep-ph/9907383](#)].

[86] A .S .Joshiipura and S .M ohanty, *Phys. Rev. D* 66, 012003 (2002), [[hep-ph/0204305](#)].

[87] J.A .G rifols, E .M asso and S .M ohanty, [hep-ph/0401144](#).

[88] SuperK am iokande C ollaboration, D .W .Liu et al., [hep-ex/0402015](#).

[89] A .V .D erbin, *Phys. Atom . Nucl.* 57, 222 (1994).

[90] TEXONO C ollaboration, H .B .Li et al., [hep-ex/0212003](#).

[91] M UNU C ollaboration, Z .D araktdchieva et al., *Phys. Lett. B* 564, 190 (2003), [[hep-ex/0304011](#)].

[92] D .Y .B ardin, S .M .B ilenky and B .Pontecorvo, *Phys. Lett. B* 32, 68 (1970).

[93] A .V .K yulduzjev, *Nucl. Phys. B* 243, 387 (1984).

[94] W .G rimus and T .Schwetz, *Nucl. Phys. B* 587, 45 (2000), [[hep-ph/0006028](#)].

[95] B orexino C ollaboration, G .A limonti et al., *A stropart. Phys.* 16, 205 (2002), [[hep-ex/0012030](#)].

[96] G .L .Fogli et al., *Phys. Rev. D* 67, 073002 (2003), [[hep-ph/0212127](#)].

[97] M .C .G onzalez-G arcia and C .P ena-G aray, [hep-ph/0306001](#).

[98] Particle D ata G roup, K .H agi w a r a et al., *Phys. Rev. D* 66, 010001 (2002).

[99] M .C .G onzalez-G arcia and M .M altoni, *Eur. Phys. J. C* 26, 417 (2003), [[hep-ph/0202218](#)].

[100] M .D o i, T .K otani, H .N ishiura, K .O kuda and E .T akasugi, *Phys. Lett. B* 102, 323 (1981).

[101] C HOOZ C ollaboration, M .A pollonio et al., *Phys. Lett. B* 466, 415 (1999), [[hep-ex/9907037](#)].

[102] J .S chechter and J .W .F .V alle, *Phys. Rev. D* 21, 309 (1980).

[103] M .F reund, *Phys. Rev. D* 64, 053003 (2001), [[hep-ph/0103300](#)].

[104] E .K .A kmedov, R .Johansson, M .L indner, T .O hlsson and T .Schwetz, [hep-ph/0402175](#).

[105] Palo Verde C ollaboration, F .Boehm et al., *Phys. Rev. D* 64, 112001 (2001), [[hep-ex/0107009](#)].

[106] P .H uber, M .L indner, M .R olinec, T .Schwetz and W .W inter, [hep-ph/0403068](#).

[107] E .K .A kmedov, M .A .T ortola and J .W .F .V alle, [hep-ph/0404083](#), JHEP in press.

[108] M .B lennow, T .O hlsson and H .S nellen, *Phys. Rev. D* 69, 073006 (2004), [[hep-ph/0311098](#)].

[109] C .Y anagisawa, P roc. of InternationalW orkshop on A stroparticle and H igh E nergy P hysics, October 14 - 18, 2003, Valencia, Spain, published at JHEP, PR HEP-A HEP 2003/062, accessible from <http://i.c.uv.es/ahep/>.

[110] LSND C ollaboration, A .A guilar et al., *Phys. Rev. D* 64, 112007 (2001), [[hep-ex/0104049](#)].

[111] J .T .P eltoniem i and J .W .F .V alle, *Nucl. Phys. B* 406, 409 (1993), [[hep-ph/9302316](#)].

[112] J .T .P eltoniem i, D .T ommasini and J .W .F .V alle, *Phys. Lett. B* 298, 383 (1993).

[113] D .O .C aldwell and R .N .M ohapatra, *Phys. Rev. D* 48, 3259 (1993).

[114] KARMEN C ollaboration, B .A mbruster et al., *Phys. Rev. D* 65, 112001 (2002),

[hep-ex/0203021].

- [115] C D H S Collaboration, F . D ydak et al, Phys. Lett. B 134, 281 (1984).
- [116] Y . D eclairis et al, Nucl. Phys. B 434, 503 (1995).
- [117] M . M altoni, T . Schwetz and J. W . F . Valle, Phys. Rev. D 65, 093004 (2002), [hep-ph/0112103].
- [118] M . C . G onzalez-G arcia, M . M altoni and C . Pena-G aray, Phys. Rev. D 64, 093001 (2001), [hep-ph/0105269].
- [119] M . M altoni, T . Schwetz, M . A . Tortola and J.W . F . Valle, Nucl. Phys. B 643, 321 (2002), [hep-ph/0207157].
- [120] M . M altoni and T . Schwetz, Phys. Rev. D 68, 033020 (2003), [hep-ph/0304176].
- [121] H . Paes, L .g. Song and T . J. W eiler, Phys. Rev. D 67, 073019 (2003), [hep-ph/0209373].
- [122] M . M altoni, T . Schwetz and J.W . F . Valle, Phys. Lett. B 518, 252 (2001), [hep-ph/0107150].
- [123] E . D . C hurch, K . E itel, G . B . M ills and M . S teidl, Phys. Rev. D 66, 013001 (2002), [hep-ex/0203023].
- [124] S . M . B ilenky, C . G iunti and W . G rimus, Eur. Phys. J. C 1, 247 (1998), [hep-ph/9607372].
- [125] N . O kada and O . Y asuda, Int. J. Mod. Phys. A 12, 3669 (1997), [hep-ph/9606411].
- [126] V . D . Barger, S . Pakvasa, T . J. W eiler and K . W hisnant, Phys. Rev. D 58, 093016 (1998), [hep-ph/9806328].
- [127] S . M . B ilenky, C . G iunti, W . G rimus and T . Schwetz, Phys. Rev. D 60, 073007 (1999), [hep-ph/9903454].
- [128] O . L . G . P eres and A . Y . S m imov, Nucl. Phys. B 599, 3 (2001), [hep-ph/0011054].
- [129] C . G iunti and M . Laveder, JHEP 02, 001 (2001), [hep-ph/0010009].
- [130] W . G rimus and T . Schwetz, Eur. Phys. J. C 20, 1 (2001), [hep-ph/0102252].
- [131] M . C . G onzalez-G arcia, M . M altoni and T . Schwetz, Phys. Rev. D 68, 053007 (2003), [hep-ph/0306226].
- [132] H . M urayama and T . Y anagida, Phys. Lett. B 520, 263 (2001), [hep-ph/0010178].
- [133] G . B arenboim , L . B orissov and J . Lykken, hep-ph/0212116.
- [134] B . A mbruster et al, Phys. Rev. Lett. 90, 181804 (2003), [hep-ex/0302017].
- [135] B oone Collaboration, E . D . Z imm erman, eConfC 0209101, TH 05 (2002), [hep-ex/0211039].